Living Rev Relativ manuscript No.
(will be inserted by the editor)

Prospects for Observing and Localizing Gravitational-Wave Transients with Advanced LIGO, Advanced Virgo and KAGRA

Abbott, B. P. et al. (KAGRA Collaboration, LIGO Scientific Collaboration and Virgo Collaboration)

Received: September 7, 2017/ Accepted:

Abstract We present possible observing scenarios for the Advanced LIGO, Advanced Virgo and KAGRA gravitational-wave detectors over the next decade, with the intention of providing information to the astronomy community to facilitate planning for multi-messenger astronomy with gravitational waves. We estimate the sensitivity of the network to transient gravitational-wave signals, and study the capability of the network to determine the sky location of the source. We report our findings for gravitational-wave transients, with particular focus on gravitational-wave signals from the inspiral of binary neutron star systems, which are considered the most promising for multi-messenger astronomy. The ability to localize the sources of the detected signals depends on the geographical distribution of the detectors and their relative sensitivity, and 90% credible regions can be as large as thousands of square degrees when only two sensitive detectors are operational. Determining the sky position of a significant fraction of detected signals to areas of 5 deg^2 to 20 deg^2 requires at least three detectors of sensitivity within a factor of ~ 2 of each other and with a broad frequency bandwidth. When all detectors, including KAGRA and the third LIGO detector in India, reach design sensitivity, a significant fraction of gravitational-wave signals will be localized to a few square degrees by gravitational-wave observations alone.

Keywords Gravitational waves · Gravitational-wave detectors · Electromagnetic counterparts · Data analysis

PACS 04.30.–w · 04.80.Nn · 95.55.Ym · 95.85.Sz

The full author list and affiliations are given at the end of paper.

1 Introduction

Advanced LIGO (aLIGO) [1,2], Advanced Virgo (AdV) [3,4,5] and KAGRA [6,7] are kilometer-scale gravitational-wave (GW) detectors that are sensitive to GWs with frequencies of $\sim 20-2000$ Hz.[1] The era of GW astronomy began with the detection of GW150914, a signal from the coalescence of a binary black hole (BBH) [8]. In this article, we describe the currently projected schedule, sensitivity, and sky-localization accuracy for the GW-detector network. We discuss the past and future planned sequence of observing runs (designated O1, O2, O3, etc.) and the prospects for multi-messenger astronomy.

The purpose of this article is to provide information to the astronomy community to assist in the formulation of plans for forthcoming GW observations. In particular, we intend this article to provide the information required for assessing the features of programs for joint observation of GW events using electromagnetic, neutrino, or other facilities (e.g., [9,10,11]).

The full science of ground-based GW detectors is broad [12], and is not covered in this article. We concentrate solely on candidate GW transient signals. We place particular emphasis on the coalescence of binary neutron star (BNS) systems, which are the GW source for which electromagnetic follow-up seems most promising [13,14, 15,16]. However, we also mention BBHs, as they are the first systems to be detected [8, 17,18,19]. No electromagnetic emission is expected for vacuum BBH mergers [20], but is possible if there is surrounding material [21], for example remnants of mass lost from the parent star [22,23] or if the binary was embedded in a circumbinary disc or a common envelope [24,25,26]. For more general introductory articles on GW generation, detection and astrophysics, we point readers to [27,28,29].

Although our collaborations have amassed a great deal of experience with GW detectors and analysis, it is still difficult to make predictions for both improvements in search methods and for the rate of progress for detectors which are not yet fully installed or operational. *The scenarios of detector sensitivity evolution and observing times given here should not be considered as fixed or firm commitments.*

As the detectors' construction and commissioning progress, we intend to release updated versions of this article. This is the third version of the article, written to coincide with the close of the second observing run (O2) of the advanced-detector era. Changes with respect to the previous version [30] are given in Appendix A. Progress has been made in the commissioning of the detectors. We include projections for KAGRA for the first time; we also include results from the first observing run (O1) and currently available results from O2.

[1] LIGO is short for Laser Interferometer Gravitational-wave Observatory. KAGRA is named after the Japanese word for traditional sacred music and dance for the gods *kagura*; the name has a secondary meaning as an abbreviation for KAmioka GRavitational-wave Antenna. Virgo is not an acronym, and is not written in all caps.

2 Commissioning and Observing Phases

We divide the development of the GW observatories into three components:

Construction includes the installation and testing of the detectors. This phase ends with *acceptance* of the detectors. Acceptance means that the interferometers can lock for periods of hours: light is resonant in the arms of the interferometer with *no guaranteed GW sensitivity.* Construction incorporates several short *engineering runs* with no astrophysical output as the detectors progress towards acceptance. The aLIGO construction project ended in March 2015. The construction of AdV was completed at the end of 2016. KAGRA will be operational in its full configuration by early 2019.

Commissioning improves the detectors' performance with the goal of reaching the design sensitivity. Engineering runs in the commissioning phase allow us to understand our detectors and analyses in an observational mode; these are not intended to produce astrophysical results, but that does not preclude the possibility of this happening.[2] Rather than proceeding directly to design sensitivity before making astrophysical observations, commissioning is interleaved with *observing runs*.

Observing runs begin when the detectors have reached (and can stably maintain) a significantly improved sensitivity compared with previous operation. Observing runs will produce astrophysical results, direct detections from some GW sources and upper limits on the rates or energetics of others. During this phase, exchange of GW candidates with partners outside the LIGO Scientific Collaboration (LSC) and the Virgo Collaboration will be governed by memoranda of understanding (MOUs) [31,32]. From the start of the third observing run (O3), high-confidence GW event candidates will be released immediately to the full astronomical community. KAGRA will become a part of the global network with full data sharing, once sensitivities comparable with aLIGO and AdV are achieved.

The progress in sensitivity as a function of time will influence the duration of the observing runs that we plan at any stage. Commissioning is a complex process which involves both scheduled improvements to the detectors and tackling unexpected new problems. While our experience makes us cautiously optimistic regarding the schedule for the advanced detectors, we are targeting an order of magnitude improvement in sensitivity relative to the previous generation of detectors over a wider frequency band. Consequently, it is not possible to make concrete predictions for sensitivity or duty cycle as a function of time. We can, however, use our experience as a guide to plausible scenarios for the detector operational states that will allow us to reach the desired sensitivity. Unexpected problems could slow down the commissioning, but there is also the possibility that progress may happen faster than predicted here. The schedule of commissioning phases and observation runs will be driven by a cost–benefit analysis of the time required to make significant sensitivity improvements. More information on event rates could also change the schedule and duration of runs.

[2] The detection of GW150914 occurred in the engineering run ER8 immediately preceding the formal start of O1.

In Section 2.1 we present the commissioning plans for the aLIGO, AdV and KAGRA detectors. A summary of expected observing runs is in Section 2.2.

2.1 Commissioning and observing roadmap

The anticipated strain sensitivity evolution for aLIGO, AdV and KAGRA is shown in Figure 1. As a standard figure of merit for detector sensitivity, we use the range, the volume- and orientation-averaged distance at which a compact binary coalescence consisting of a particular mass gives a matched filter signal-to-noise ratio (SNR) of 8 in a single detector [33]. We define V_z as the orientation-averaged spacetime volume surveyed per unit detector time; for a population with a constant comoving source-frame rate density, V_z multiplied by the rate density gives the detection rate of those sources by the particular detector. We define the range R as the distance for which $(4\pi/3)R^3 = V_z$. In Table 1 we present values of R for different detector networks and binary sources. For further insight into the range, and a discussion of additional quantities such as the median and average distances to sources, please see [34]. The BNS ranges, assuming two $1.4\,M_\odot$ neutron stars, for the various stages of the expected evolution are provided in Figure 1, and the BNS and BBH ranges are quoted in Table 1.

Table 1 Plausible target detector sensitivities. The different phases match those in Figure 1. We quote the range, the average distance to which a signal could be detected, for a $1.4\,M_\odot$+$1.4\,M_\odot$ binary neutron star (BNS) system and a $30\,M_\odot$+$30\,M_\odot$ binary black hole (BBH) system.

	LIGO		Virgo		KAGRA	
	BNS range/Mpc	BBH range/Mpc	BNS range/Mpc	BBH range/Mpc	BNS range/Mpc	BBH range/Mpc
Early	40 – 80	415 – 775	20 – 65	220 – 615	8 – 25	80 – 250
Mid	80 – 120	775 – 1110	65 – 85	615 – 790	25 – 40	250 – 405
Late	120 – 170	1110 – 1490	65 – 115	610 – 1030	40 – 140	405 – 1270
Design	190	1640	125	1130	140	1270

There are currently two operational aLIGO detectors. The original plan called for three identical 4-km interferometers, two at Hanford (H1 and H2) and one at Livingston (L1). In 2011, the LIGO Lab and IndIGO consortium in India proposed installing one of the aLIGO Hanford detectors (H2) at a new observatory in India (LIGO-India) [35]. In early 2015, LIGO Laboratory placed the H2 interferometer in long-term storage for use in India. The Government of India granted in-principle approval to LIGO-India in February 2016.

The first observations with aLIGO have been made. O1 formally began 18 September 2015 and ended 12 January 2016; however, data from the surrounding engineering periods were of sufficient quality to be included in the analysis, and hence the first observations span 12 September 2015 to 19 January 2016. The run involved the H1 and L1 detectors; the detectors were not at full design sensitivity [36]. We aimed for a BNS range of 40 – 80 Mpc for both instruments (see Figure 1), and achieved a

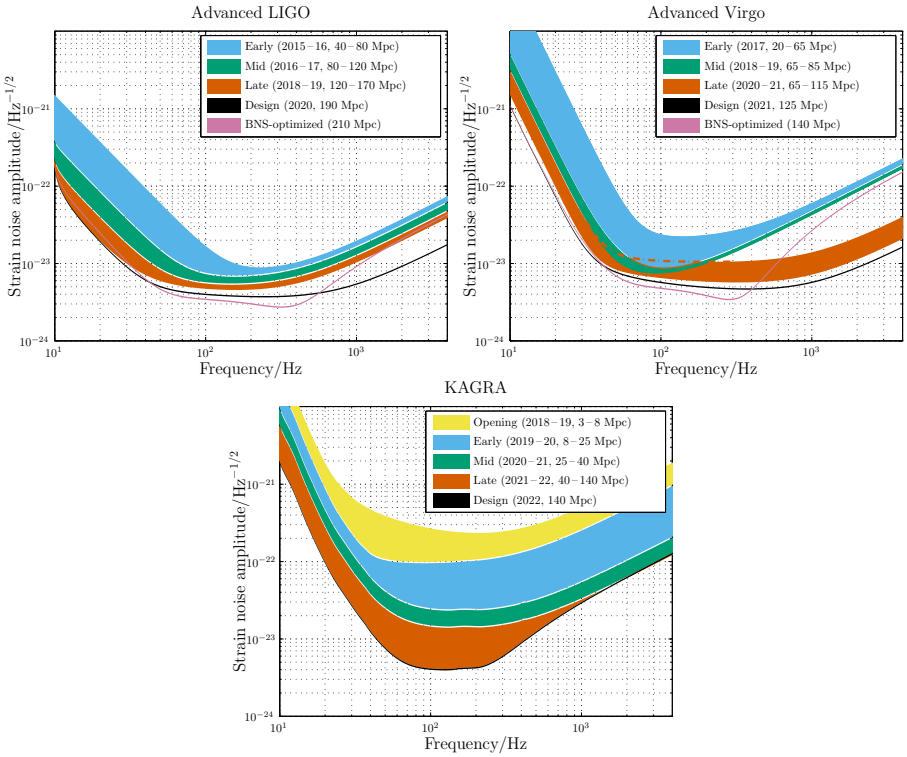

Fig. 1 Regions of aLIGO (*top left*), AdV (*top right*) and KAGRA (*bottom*) target strain sensitivities as a function of frequency. The binary neutron star (BNS) range, the average distance to which these signals could be detected, is given in megaparsec. Current notions of the progression of sensitivity are given for early, mid and late commissioning phases, as well as the final design sensitivity target and the BNS-optimized sensitivity. While both dates and sensitivity curves are subject to change, the overall progression represents our best current estimates.

60 – 80 Mpc range. Subsequent observing runs have increasing duration and sensitivity. O2 began 30 November 2016, transitioning from the preceding engineering run which began at the end of October, and ended 25 August 2017. The achieved sensitivity across the run has been typically in the range 60 – 100 Mpc [19]. Assuming that no unexpected obstacles are encountered, the aLIGO detectors are expected to achieve a 190 Mpc BNS range by 2020. After the first observing runs, it might be desirable to optimize the detector sensitivity for a specific class of astrophysical signals, such as BNSs. The BNS range may then become 210 Mpc. The sensitivity for each of these stages is shown in Figure 1.

The H2 detector will be installed in India once the LIGO-India Observatory is completed, and will be configured to be identical to the H1 and L1 detectors. We refer to the detector in this state as I1 (rather than H2). Operation at the same level as the H1 and L1 detectors is anticipated for no earlier than 2024.

The AdV interferometer (V1) [4] officially joined O2 on 1 August 2017. We aimed for an early step with sensitivity corresponding to a BNS range of 20 – 65 Mpc;

however, AdV is currently using steel wires to suspend the test masses, instead of fused silica fibers. This limits the highest possible BNS range in O2 to 40 – 60 Mpc; the BNS range achieved to date is 25 – 30 Mpc. Fused silica fibers will be reinstalled after O2. Commissioning is expected to bring the AdV BNS range to 65 – 85 Mpc in 2018 – 2019. A configuration upgrade at this point will allow the range to increase to approximately 65 – 115 Mpc in 2020. The final design sensitivity, with a BNS range of 125 Mpc, is anticipated circa 2021. The corresponding BNS-optimized range would be 140 Mpc. The sensitivity curves for the various AdV configurations are shown in Figure 1.

The KAGRA detector (K1) [6,7] is located at the Kamioka underground site. The first operation of a detector in an initial configuration with a simple Michelson interferometer occurred in March 2016. The detector is now being upgraded to its baseline design configuration. Initial operation at room temperature is expected in 2018. Subsequently, the detector will be cryogenically cooled to reduce thermal noise. Early cryogenic observations may come in 2019 – 2020 with a range of 8 – 25 Mpc. Since sensitivity will lag behind that of aLIGO and AdV, observing runs are planned to be short to allow commissioning to proceed as quickly as possible; longer observing runs may begin when the detector nears design sensitivity of 140 Mpc. The exact timing of observations has yet to be decided, but it is currently intended to have a three-month observing run in early 2020, and a six-month run at the start of 2021. The sensitivity curves for the various KAGRA commissioning stages are shown in Figure 1.

GEO 600 [37,38] will continue to operate as a GW detector beyond O3 as techniques for improving the sensitivity at high frequency are investigated [39]. At its current sensitivity, it is unlikely to contribute to detections, but with a deliberate focus on high frequency narrow band sensitivity at a few kilohertz, GEO 600 may contribute to the understanding of BNS merger physics, as well as sky localization for such systems, by around 2021. In the meantime, it will continue observing with frequent commissioning and instrument science investigations related to increasing laser power [38,40,41,42] and optical squeezing [43,44,45].

Finally, further upgrades to the LIGO and Virgo detectors, within their existing facilities (e.g., [46,47,48]) as well as future third-generation observatories (for example, the Einstein Telescope [49,50,51] or Cosmic Explorer [52]) are envisioned in the future. It is also possible that for some sources, there could be multiband gravitational-wave observations, where detection with a space-borne detector like the Laser Interferometer Space Antenna (LISA) [53,54] could provide early warning and sky localization [55], as well as additional information on system parameters [56], formation mechanisms [57,58,59] and tests of general relativity [60]. These potential future developments are beyond the scope of this paper.

2.2 Past and envisioned observing schedule

Keeping in mind the important caveats about commissioning affecting the scheduling and length of observing runs, the following are plausible scenarios for the operation of the ground-based GW detector network over the next decade:

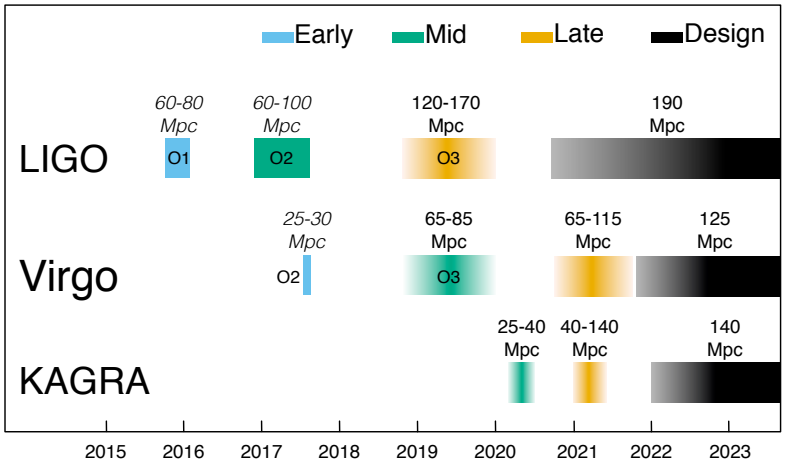

Fig. 2 The planned sensitivity evolution and observing runs of the aLIGO, AdV and KAGRA detectors over the coming years. The colored bars show the observing runs, with the expected sensitivities given by the data in Figure 1 for future runs, and the achieved sensitivities in O1 and in O2. There is significant uncertainty in the start and end times of planned the observing runs, especially for those further in the future, and these could move forward or backwards relative to what is shown above. The plan is summarised in Section 2.2.

2015 – 2016 (O1) A four-month run (12 September 2015 – 19 January 2016) with the two-detector H1L1 network at early aLIGO sensitivity (60 – 80 Mpc BNS range). This is now complete.

2016 – 2017 (O2) A nine-month run with H1L1, joined by V1 for the final month. O2 began on 30 November 2016, with AdV joining 1 August 2017 and ended on 25 August 2017. The expected aLIGO range was 80 – 120 Mpc, and the achieved range was in the region of 60 – 100 Mpc; the expected AdV range was 20 – 65 Mpc, and the initial range was 25 – 30 Mpc

2018 – 2019 (O3) A year-long run with H1L1 at 120 – 170 Mpc and with V1 at 65 – 85 Mpc beginning about a year after the end of O2.

2020+ Three-detector network with H1L1 at full sensitivity of 190 Mpc and V1 at 65 – 115 Mpc, later increasing to design sensitivity of 125 Mpc.

2024+ H1L1V1K1I1 network at full sensitivity (aLIGO at 190 Mpc, AdV at 125 Mpc and KAGRA at 140 Mpc). Including more detectors improves sky localization [61, 62, 63, 64] as well as the fraction of coincident observational time. 2024 is the earliest time we imagine LIGO-India could be operational.

This timeline is summarized in Figure 2; we do not include observing runs with LIGO-India yet, as these are still to be decided. Additionally, GEO 600 will continue observing, with frequent commissioning breaks, during this period. The observational implications of these scenarios are discussed in Section 4.

3 Searches for Gravitational-Wave Transients

Data from GW detectors are searched for many types of possible signals [12]. Here we focus on signals from compact binary coalescences (CBCs) and on generic transient or *burst* signals. CBCs include BNS, neutron star–black hole (NS–BH) and BBH systems.

Observational results of searches for transient signals are reported in [65, 18, 66, 67, 68, 69, 19]. The O1 results include two clear detections GW150914 [8] and GW151226 [17], and a lower significance candidate LVT151012 [65, 18]. All three originate from BBH coalescences [70, 18]. No other transient sources have been identified in O1 [68, 67, 71]. The first detection of O2 has been announced: GW170104 is an additional BBH coalescence [19].

The rate of BNS coalescences is uncertain [72]. For this work we adopt the estimates of [73], which predicts the rate density to lie between 10^{-8} – 10^{-5} Mpc^{-3} yr^{-1}, with a most plausible value of 10^{-6} Mpc^{-3} yr^{-1}; this corresponds to 0.3 – 300 signals above an SNR of 8 per year of observation for a single aLIGO detector at final sensitivity, and a best estimate of 30 BNS signals per year [73]. Rate estimation remains an active area of research (e.g., [74, 75, 76, 77, 78, 79]), and will be informed by the number of detections (or lack thereof) in observing runs. The non-detection of BNSs in O1 places a 90% upper limit on the merger rate of 1.3×10^{-5} Mpc^{-3} yr^{-1}, consistent with all but the most optimistic astrophysical models [68].

While the rates per unit volume of NS–BH and BBH mergers are expected to be lower than for BNSs, the distance to which they can be observed is larger. Consequently, the predicted observable rates are comparable [73, 80, 81, 82]. From our observations of BBHs, we infer that their rate of mergers is in the range $\sim 1.2 \times 10^{-8}$ – 2.13×10^{-7} Mpc^{-3} yr^{-1} [19]. The non-detection of NS–BHs in O1 allows us to place a 90% upper limit of the merger rate of 3.6×10^{-6} Mpc^{-3} yr^{-1}, assuming $1.4M_{\odot} + 5M_{\odot}$ binaries with isotropically distributed spins [68]; the upper limit on the rate decreases for higher mass black holes. Expected detection rates for other transient sources are lower and/or less well constrained.

The gravitational waveform from the inspiral phase of a BNS coalescence is well modeled and matched filtering can be used to search for signals [83, 84, 85, 86, 65, 87]. For systems containing black holes, or in which the component spin is significant, uncertainties in the waveform model can reduce the sensitivity of the search [88, 89, 90, 91, 92, 93, 94, 95].

Searches for bursts make few assumptions on the signal morphology, using time–frequency decompositions to identify statistically significant excess-power transients in the data. Burst searches generally perform best for short-duration signals ($\lesssim 1$ s), although search development remains an area of active research (e.g., [96, 97, 98, 99, 100, 101, 102, 103, 104]); their astrophysical targets include core-collapse supernovae, magnetar flares, BBH coalescences, cosmic string cusps, and, possibly, as-yet-unknown systems.

In the era of advanced detectors, we are searching in *near real-time* for CBC and burst signals for the purpose of rapidly identifying event candidates. A prompt notice of a potential GW transient might enable follow-up observations in the electromagnetic spectrum.

A first follow-up program including low-latency analysis, event candidate selection, position reconstruction and the sending of alerts to several observing partners (optical, X-ray, and radio) was implemented and exercised during the 2009 – 2010 LIGO–Virgo science run [105, 106, 107]. Latencies of less than 1 hour were achieved.

In the present follow-up program, the LSC and Virgo distribute the times and sky localizations using the Gamma-ray Coordinates Network (GCN) system, widely used in the astronomical community for the multiwavelength follow-up of gamma-ray bursts.[3] Messages are sent as machine-readable GCN Notices and as prose GCN Circulars, and partners communicate the results of observations using GCN Circulars. A shared infrastructure, including a database of results, allows observing partners to announce, coordinate and visualize the coverage of their observations.[4] Prior to O1, 74 teams signed MOUs to participate in the electromagnetic follow-up program, and for the first event candidate later confirmed as GW150914, 63 were operational and covered the full electromagnetic spectrum [9, 108]. For the first observations with the advanced detectors, thorough checks were performed before alerts were released, resulting in latencies much greater than 1 hour. We expect this latency to be improved in the future as we gain experience with the instruments, and aim for automatic alerts being sent out with only a few minutes latency; continued checks may lead to retractions of some of these low-latency alerts. In the case of GW150914, 25 teams responded to the GW alert and operated ground- and space-based instruments spanning 19 orders of magnitude in electromagnetic wavelength [109, 110, 111, 112, 113, 114, 115, 116, 117, 118, 119, 120, 121, 121, 122, 123]. Analyses of archival data were also performed [124, 125]. No significant electromagnetic counterpart and no afterglow emission was found in optical, ultraviolet, X-rays, or GeV gamma rays. The weak transient found in Fermi-GBM data 0.4 s after GW150914 [111, 126] was not confirmed by other instruments like INTEGRAL SPI-ACS [113], AGILE [125] or any other experiments of the InterPlanetary Network [116]. Models have been proposed to tentatively explain electromagnetic emission from BBHs, but there is no clear favorite as yet [127, 25, 22, 23, 24, 26, 128, 129, 130, 131, 132, 133, 134, 135]. There was no significant neutrino emission temporally and spatially coincident with the event, and all detected neutrino candidates are consistent with the background [10, 136, 137, 138, 139].

A similar follow-up campaign was performed for the event candidate later confirmed as GW151226 and no electromagnetic counterpart has been reported [140, 141, 118, 142, 143, 144, 115, 145, 146]. LVT151012 was only identified in an offline search [65], as an online CBC search for BBHs was not running at the time, and therefore no low-latency alert was sent. Nevertheless, some searching of archival data has been done, and no confident counterparts have been found [142]. As for GW150914, no significant neutrino counterpart was found in coincidence with either

[3] Details of the GCN are available from gcn.gsfc.nasa.gov, and archives of messages for GW150914 (gcn.gsfc.nasa.gov/other/GW150914.gcn3), LVT151012 (gcn.gsfc.nasa.gov/other/G197392.gcn3), GW151226 (gcn.gsfc.nasa.gov/other/G211117.gcn3) and GW170104 (gcn.gsfc.nasa.gov/other/G268556.gcn3) are now publicly available.

[4] More details about the technical aspects of the follow-up program are available from gw-astronomy.org/wiki/LV_EM/TechInfo. Scientists interested in joining the follow-up program are encouraged to follow the guidelines at www.ligo.org/scientists/GWEMalerts.php.

event [11,136,137,138,139]. A lack of counterparts is unsurprising given our current understanding of BBHs.

During O2, for GW170104, an alert with initial localization was sent in under 7 hours, and was followed up by observatories spanning the electromagnetic spectrum as well as neutrinos [19]. No confirmed counterpart has yet been reported for this BBH [147,148,149,150,151,139,152].

Increased detection confidence, improved sky localization, and identification of host galaxy and redshift are just some of the benefits of joint GW–electromagnetic observations. With this in mind, we focus on two points of particular relevance for follow-up of GW events: the source localization afforded by a GW network as well as the relationship between signal significance, or false alarm rate (FAR), and source localization.

3.1 Detection and false alarm rates

Detection pipelines search the data looking for signal-like features. Candidate triggers flagged by a pipeline are assigned a detection statistic to quantify how signal-like they are. For CBC searches, this involves matching a bank of waveform templates [153, 154,155,156,157,158,159,160,85,161,162] to the data [65,18]; for burst searches, requirements on waveform morphology are relaxed, but coherence of the signal in multiple detectors is required [66,67]. The detection statistic is used to rank candidates; we assess significance by comparing results with those from an estimated background distribution of noise triggers. It is difficult to theoretically model the behaviour of non-Gaussian noise, and therefore the distribution must be estimated from the data [163, 164,165,166,167,168,65,18,66,67,169]. From the background noise distribution we can map a value of the detection statistic to a FAR, the expected rate of triggers with detection statistics equal to or greater than that value, assuming that the data contain no signals. While each pipeline has its own detection statistic, they all compute a FAR, making it easy to compare results. The FAR, combined with the observation time, may then be used to calculate a p-value, the probability of there being at least one noise trigger with a FAR this small or smaller in the observed time.[5] As the FAR or p-value of a trigger decreases, it becomes more significant, and more likely to be a genuine astrophysical signal.

The rate of noise triggers above a given SNR depends critically upon the data quality of the advanced detectors; non-stationary transients or *glitches* [172,173,174] produce an elevated background of loud triggers. Over 200,000 auxiliary channels record data on instrumental and environmental conditions [175,174]. These channels act as witnesses of disturbances that may couple into the GW channel. An intensive study of the data quality is used to veto stretches of acquired data ranging from

[5] The p-value is distinct from the probability that a trigger is not a real astrophysical GW signal. The p-value assumes that the data contain no signals, whereas the probability of there being a GW must include the hypothesis that there is an astrophysical signal. To calculate the probability that a trigger is a real signal (or not) requires an extra layer of inference, folding in both our knowledge of the distribution of triggers, assumptions about the signal distribution (such as that sources are uniformly distributed in volume), and knowledge and assumptions about the merger rate per unit volume for a class of sources. A method for doing this is described in [170,171,18].

seconds to hours in duration. When a significant problem with the data is identified or a known instrumental issue affects the searches' background, the contaminated data are removed from the analysis data set. Our experience to date is that this removes a small percentage of the data; for example, in O1 vetoes removed less than 5% of the coincident data from the CBC analysis, with a single intermittent instrumental problem accounting for 4.65% of that total [174, 18, 67]. For low-mass CBC searches, the waveforms are well modeled, and signal consistency tests reduce the background significantly [176, 177, 178]. For burst sources which are not well modeled, or which spend only a short time in the detectors' sensitive band, it is more difficult to distinguish between the signal and a glitch, and so a reduction of the FAR comes at a higher cost in terms of reduced detection efficiency (or livetime if more vetoes are used).

Search pipelines are run both online, analysing data as soon as they are available in order to provide low-latency alerts of interesting triggers, and offline, taking advantage of improved calibration of the data and additional information regarding data quality. In Figure 3, we show the offline transient search results for O1.[6]

For CBC, we show the cumulative number of triggers at a given FAR for two pipelines: PyCBC [180, 178] and GstLAL [181, 182, 168]. In the ongoing O2 analysis, PyCBC uses an improved detection statistic [169]. GW150914, LVT151012 and GW151226 are visible in both the GstLAL and PyCBC results [65, 18] shown in Figure 3.

For bursts, we show distributions for COHERENT WAVE BURST (CWB) [183, 96], Omicron–LALINFERENCEBURST (OLIB) [184] and BAYESWAVE [102, 185]. The CWB analysis is split into two frequency bands, above and below 1024 Hz. The OLIB search is split into two bins, based upon the quality factor Q of the sine–Gaussian it uses to model the signal; no triggers were identified by the low-Q search. BAYESWAVE is run as a follow-up to triggers identified by CWB [104], and hence is not completely independent. GW150914 was identified by all three search algorithms [66, 67].

For CBC signals, we conservatively estimate that a network SNR threshold of $\rho_c \simeq 12$ is required for a FAR below $\sim 10^{-2}$ yr^{-1} in the advanced-detector era [186, 30, 187]. A combined SNR of 12 corresponds to a single-detector SNR of 8.5 in each of two detectors, or 7 in each of three detectors (assuming an orientation and sky location for which the detectors have equal sensitivity). The exact threshold will depend upon data quality in each observing run as well as the mass of the source; in O1, we found that the threshold SNR was lower, around 10.

3.2 Localization

Following the detection of a GW transient posterior probability distributions for the position are constructed following a Bayesian framework [188, 102, 189, 70], with information for the sky localization coming from the time of arrival, plus the phase and amplitude of the GW.

[6] Strain data from the three probable events in O1 and for GW170104 in O2 are publicly available from the LIGO Open Science Center losc.ligo.org [179]. Full data from observing runs will be added in the future.

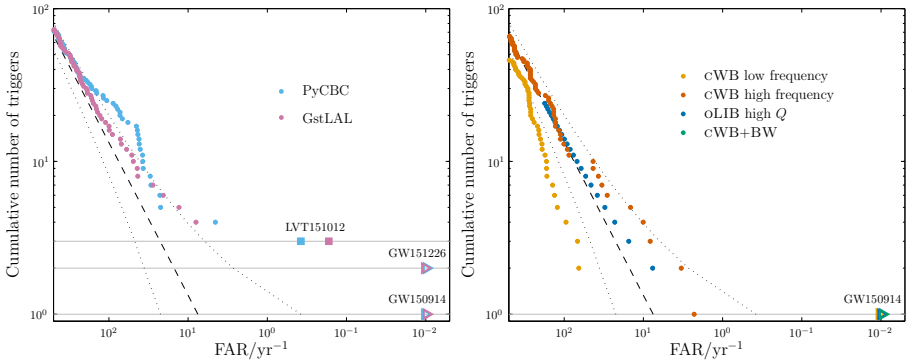

Fig. 3 Offline transient search results for the first observing run: the cumulative number of triggers with false alarm rates (FARs) smaller than the abscissa value. The dashed line shows the expected noise-only distribution, and the dotted lines show the 90% confidence interval assuming no signals. Potential signals are identified by having smaller FARs than expected. The plots are truncated at a minimum FAR of 10^{-2} yr^{-1}. *Left*: Compact binary coalescence search results [18,68]. We show results from two search algorithms, GstLAL [181,182,168] and PyCBC [180,178]. The most significant triggers for both are LVT151012, GW151226 and GW150914; GW150914 and GW151226 have FARs less than 10^{-2} yr^{-1}. *Right*: Burst search results [67]. We show results from three search algorithms, COHERENT WAVE BURST (cWB) [183,96], Omicron–LALINFERENCEBURST (oLIB) [184] and BAYESWAVE follow-up of cWB (cWB+BW) [104]. All three found GW150914 (the only cWB trigger above BAYESWAVE follow-up threshold) with a FAR less than 10^{-2} yr^{-1}. GW151226 and LVT151012 fall below the burst search's detection threshold.

An intuitive understanding of localization can be gained by considering triangulation using the observed time delays between sites [190,191]. The effective single-site timing accuracy is approximately

$$\sigma_t = \frac{1}{2\pi\rho\sigma_f}\,, \tag{1}$$

where ρ is the SNR in the given detector and σ_f is the effective bandwidth of the signal in the detector, typically of order 100 Hz. Thus a typical timing accuracy is on the order of 10^{-4} s (about $1/100$ of the 10 ms light travel time between sites). This sets the localization scale. The simple model of Equation (1) ignores many other relevant issues such as information from the signal amplitudes and phases across the detector network, uncertainty in the emitted gravitational waveform, instrumental calibration accuracies, and correlation of sky location with other binary parameters [190,192,193, 194,62,63,195,187,189]. While many of these affect the measurement of the time of arrival in individual detectors, such factors are largely common between two similar detectors, so the time difference between the two detectors is relatively uncorrelated with these additional parameters.

The timing-triangulation approach underestimates how well a source can be localized, since it does not include all the relevant information. Its predictions can be improved by introducing the requirement of phase consistency between detectors [196]: it always performs poorly for a two-detector network, but, with the inclusion of phase coherence, can provide an estimate for the average performance of a three-detector network [187].

Source localization using only timing for a two-site network yields an annulus on the sky; see Figure 4. Additional information such as signal amplitude and phase, and precession effects resolve this to only parts of the annulus, but even then sources will only be localized to regions of hundreds to thousands of square degrees [195, 187]. An example of a two-detector BNS localization is shown in Figure 5. The posterior probability distribution is primarily distributed along a ring, but this ring is broken, such that there are clear maxima.

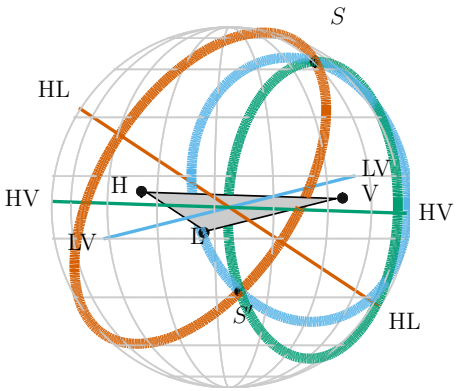

Fig. 4 Source localization by timing triangulation for the aLIGO–AdV network. The locations of the three detectors are indicated by black dots, with LIGO Hanford labeled H, LIGO Livingston as L, and Virgo as V. The locus of constant time delay (with associated timing uncertainty) between two detectors forms an annulus on the sky concentric about the baseline between the two sites (labeled by the two detectors). For three detectors, these annuli may intersect in two locations. One is centered on the true source direction (S), while the other (S') is its mirror image with respect to the geometrical plane passing through the three sites. For four or more detectors there is a unique intersection region of all of the annuli. Figure adapted from [197].

For three detectors, the time delays restrict the source to two sky regions which are mirror images with respect to the plane passing through the three sites. It is often possible to eliminate one of these regions by requiring consistent amplitudes in all detectors. For signals just above the detection threshold, this typically yields regions with areas of several tens to hundreds of square degrees. If there is significant difference in sensitivity between detectors, the source is less well localized and we may be left with the majority of the annulus on the sky determined by the two most sensitive detectors. With four or more detectors, timing information alone is sufficient to localize to a single sky region, and the additional baselines help to limit the region to under 10 deg^2 for some signals.

From Equation (1), it follows that the *linear* size of the localization ellipse scales inversely with the SNR of the signal and the frequency bandwidth of the signal in the detector [187]. For GWs that sweep across the band of the detector, such as CBC signals, the effective bandwidth is ~ 100 Hz, determined by the most sensitive frequencies of the detector. Higher mass CBC systems merge at lower frequencies and so have a smaller effective bandwidth. For burst transients, the bandwidth σ_f depends on the specific signal. For example, GWs emitted by various processes in core-collapse

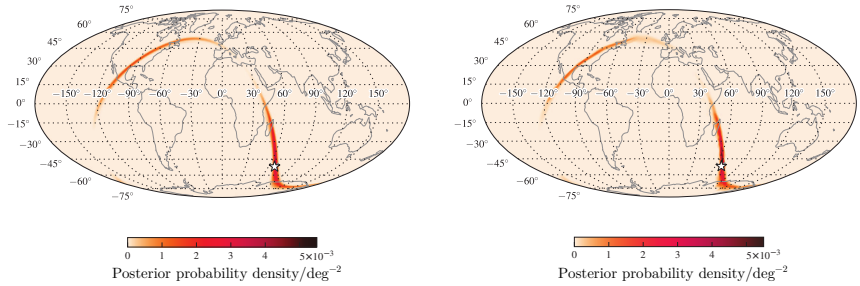

Fig. 5 Posterior probability density for sky location for an example simulated binary neutron star coalescence observed with a two-detector network. *Left*: Localization produced by the low-latency BAYESTAR code [195,189]. *Right*: Localization produced by the higher-latency LALINFERENCE [188] (neglecting spin), which also produces posterior estimates for other parameters. These algorithms are discussed in Section 3.2.1, and agreement between them shows that the low-latency localization is comparable to the one produced by the higher-latency pipelines. The star indicates the true source location. The source is at a distance of 266 Mpc and has a network signal-to-noise ratio of $\rho_c = 13.2$ using a noise curve appropriate for the first aLIGO run (O1, see Section 4.1). The plot is a Mollweide projection in geographic coordinates. Figure reproduced from [187]; further mock sky localizations for the first two observing runs can be found at www.ligo.org/scientists/first2years/ for binary neutron star signals and www.ligo.org/scientists/burst-first2years/ for burst signals.

supernovae are anticipated to have relatively large bandwidths, between 150 – 500 Hz [198,199,200,201], largely independent of detector configuration. By contrast, the sky localization region for narrowband burst signals may consist of multiple disconnected regions and exhibit fringing features; see for example [61,105,202].

In addition to localizing sources on the sky, for CBC signals it is possible to provide distance estimates, since the waveform amplitude is inversely proportional to the luminosity distance [188,70]. Uncertainty in distance measurement is dominated by the degeneracy with the binary's inclination, which also determines the signal amplitude [203,204,205]. The degeneracy can be broken by observing with more non co-aligned detectors, or if precession of the orbital plane can be observed [206,207, 208], but this is not expected for slowly spinning BNS [209]. Distance information can further aid the hunt for counterparts, particularly if the the localization can be used together with galaxy catalogs [63,210,211,212,213].

Some GW searches are triggered by electromagnetic observations, and in these cases localization information is known *a priori*. For example, in GW searches triggered by gamma-ray bursts [214,215,216,69] the triggering space-based telescope provides the localization. The detection of a GW transient associated with a gamma-ray burst would provide strong evidence for the burst progenitor; for example, BNS mergers are considered the likely progenitors of most short gamma-ray bursts. Other possible targets for these externally-triggered GW searches could be electromagnetic or neutrino emission from Galactic core-collapse supernovae. It is therefore of great scientific value to have telescopes capable of observing the high-energy spectrum operating during the advanced-detector era (and beyond). Furthermore, the rapid identification of a GW counterpart to such a trigger could prompt further spectroscopic studies and longer, deeper follow-up in different wavelengths that may not always be done in response to gamma-ray bursts. This is particularly important for gamma-

ray bursts with larger sky localization uncertainties, such as those reported by the Fermi-GBM, which are not followed up as frequently as bursts reported by Swift or Fermi-LAT. All GW data are stored permanently, so that it is possible to perform retroactive analyses at any time.

3.2.1 Localization of binary neutron star coalescences

Providing prompt localizations for GW signals helps to maximise the chance that electromagnetic observatories can catch a counterpart. Localizations are produced at several different latencies, with updates coming from more computationally expensive algorithms that refine our understanding of the source.

For CBC signals, rapid localization is performed using BAYESTAR [189], a Bayesian parameter-estimation code that computes source location using output from the detection pipeline. It can produce sky localizations (as in Figure 5) with latencies of only a few seconds. A similar approach to low-latency localization has been separately developed by [217], which find results consistent with BAYESTAR. BAYESTAR can also provide distance estimates [213]. These can be easily communicated as an additional component of the sky localization: for each line of sight, the distance posterior probability is approximated as a Gaussian multiplied by the distance squared [213, 218].[7] Results from BAYESTAR are shared with partners at low latency for prompt follow-up efforts.

At higher latency, CBC parameter estimation is performed using the stochastic sampling algorithms of LALINFERENCE [188]. LALINFERENCE constructs posterior probability distributions for system parameters (not just location like BAYESTAR, but also mass, orientation, etc. [205, 70]) by matching GW templates to the detector strain [203, 219]. Computing these waveforms is computationally expensive; this expense increases as the detectors' low-frequency sensitivity improves and waveforms must be computed down to lower frequencies. The quickest LALINFERENCE BNS follow-up is computed using waveforms that do not include the full effects of component spins [195, 187, 19], localizations can then be reported with latency of hours to a couple of days. Parameter estimation is then performed using more accurate waveform approximates (those that include fuller effects of spin precession) [209, 220, 19]. Provided that BNSs are slowly spinning [221], the restrictions on the spins should cause negligible difference between the mid-latency LALINFERENCE and the high-latency fully spinning LALINFERENCE localizations [209]. Methods of reducing the computational cost are actively being investigated (e.g., [222, 223, 224, 225, 226]).

There is negligible difference between the low-latency BAYESTAR and the LALINFERENCE analyses if the BNS signal is loud enough to produce a trigger in all detectors: if it is not, LALINFERENCE could give a more precise localization, as it still uses strain data from the non-triggered detector [195, 189]. However, in preparation for the start of joint three-detector observations in O2, the online CBC pipelines and BAYESTAR have been enhanced to capture and make use of sub-threshold signals in all detectors. Consequently, there should be negligible difference between the low-latency

[7] A data release of example three-dimension localizations in this format, constructed using results from BAYESTAR and LALINFERENCE for BNS signals, is available from dcc.ligo.org/P1500071/public/html.

BAYESTAR the and LALINFERENCE localizations even for events that register weakly in one or more detectors.

Sky localization results from an astrophysically motivated population of BNS signals, assuming a detection threshold of a SNR of 12, are shown in Figure 6 [195, 187]. Results are quantified using the 90% credible region $\mathrm{CR}_{0.9}$, the smallest area enclosing 90% of the total posterior probability, and the searched area A_*, the area of the smallest credible region that encompasses the true position [227]: $\mathrm{CR}_{0.9}$ gives the area of the sky that must be covered to expect a 90% chance of including the source location, and A_* gives the area that would be viewed before the true location is found using the given sky localization. Results from both the low-latency BAYESTAR and mid-latency LALINFERENCE analyses are shown. These are discussed further in Section 4.1 and Section 4.2. The two-detector localizations are slightly poorer in O2 than in O1. This is because although the detectors improve in sensitivity at every frequency, with the assumed noise curves the BNS signal bandwidth is lower in O2 for a given SNR because of enhanced sensitivity at low frequencies [195]. Sky localization improves with the expansion of the detector network [228,61,62,64,229].

Observing with more non co-aligned detectors will help constrain the distance of the events [62,64]. For the BNS signals from the sky-localization studies, the average fractional uncertainty, defined as the posterior standard deviation divided by the mean, is $\sim 0.25-0.30$ [187,209].

LALINFERENCE also has the ability to include the effects of the detectors' calibration uncertainty on parameter estimation [70,18]. Calibration is refined as additional measurements are taken, hence sky localization can improve as uncertainty is reduced. Initial results for GW150914 assumed a calibration uncertainty of 10% for the amplitude of the GW strain and 10 deg for its phase [230]. Incorporating this calibration uncertainty into the analysis, the 90% credible area was 610 deg^2 [70]. At the end of O1, the calibration uncertainty had been improved, such that the 90% credible area was 230 deg^2 [18]. If the detectors were assumed to be perfectly calibrated, such that calibration uncertainty could be ignored, the 90% credible area would be 150 deg^2. Sky localization is particularly sensitive to calibration uncertainty and distance is less affected. For GW150914, the initial distance estimate was 410^{+160}_{-180} Mpc [70], the estimate at the end of the run was 420^{+150}_{-180} Mpc, and the equivalent result without calibration uncertainty was 420^{+140}_{-170} Mpc [18]. The effects of calibration uncertainty depend upon the signal's SNR and position of the source relative to the detectors. For GW151226, LVT151012 GW170104, there is negligible difference between the sky areas or distances with and without calibration uncertainty (using the final calibration) [18,19].

3.2.2 Localization of bursts

Sky localizations are also produced for burst triggers and distributed for follow up. The lowest latency burst sky localizations are produced as part of the CWB detection pipeline [96,183]. Sky localizations are produced using a constrained likelihood algorithm that coherently combines data from all the detectors. The CWB sky localizations are calculated with a latency of a few minutes; following detection, further parameter-estimation codes analyze the data.

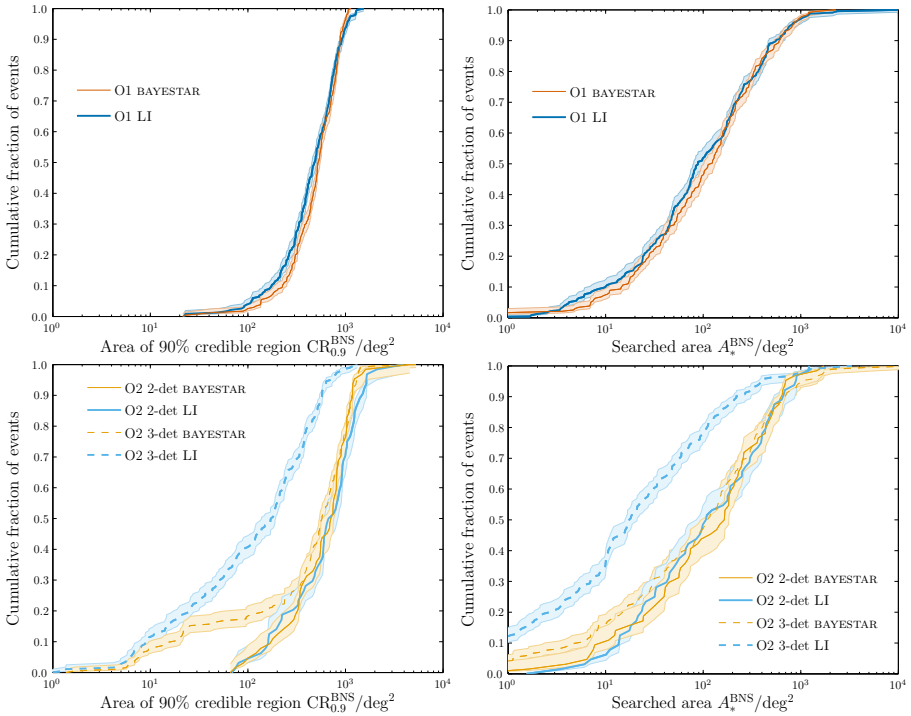

Fig. 6 Anticipated binary neutron star sky localization during the first two observing runs (*top*: O1, see Section 4.1; *bottom*: O2, see Section 4.2). Detector sensitivities were taken to be in the middle of the early (for aLIGO in O1 and AdV in O2) and mid (for aLIGO in O2) bands of Figure 1. The plots show the cumulative fractions of events with sky-localization areas smaller than the abscissa value. *Left*: Sky area of 90% credible region $\mathrm{CR}_{0.9}^{\mathrm{BNS}}$, the (smallest) area enclosing 90% of the total posterior probability. *Right*: Searched area A_*^{BNS}, the area of the smallest credible region containing the true position. Results are shown for the low-latency BAYESTAR [189] and higher-latency (neglecting spin) LALINFERENCE (LI) [188] codes. The O2 results are divided into those where two detectors (2-det) are operating in coincidence, and those where three detectors (3-det) are operating: assuming a duty cycle of 70 – 75% for each instrument, the two-detector network would be operating for 42 – 44% of the total time and the three-detector network 34 – 42% of the time. The shaded areas indicate the 68% confidence intervals on the cumulative distributions. A detection threshold of a signal-to-noise ratio of 12 is used and results are taken from [187, 195].

At higher latency, burst signals are analyzed by LALINFERENCEBURST (LIB), a stochastic sampling algorithm similar to the LALINFERENCE code used to reconstruct CBC signals [188], and BAYESWAVE, a reversible jump Markov-chain Monte Carlo algorithm that models both signals and glitches [102]. LIB uses sine–Gaussian waveforms (in place of the CBC templates used by LALINFERENCE), and can produce sky localizations in a few hours. BAYESWAVE uses a variable number of sine–Gaussian wavelets to model a signal and glitches while also fitting for the noise spectrum using BAYESLINE [185]; it produces sky localizations with a latency of a few days.

The sky-localization performance of burst algorithms depends upon the type of signal. Studies of burst localization using BAYESWAVE in the first year of the advanced-detector era, and using CWB and LIB in the first two years have been completed in [231] and [202], respectively. These assumed sensitivities in the middle

of the early band for aLIGO in O1, and in the middle of the mid band for aLIGO and the early band for AdV in O2. Sky localization was quantified by the searched area. For the cWB and LIB pipelines an approximate FAR threshold of 1 yr^{-1} was used to select events; BayesWave was run as a follow-up to triggers identified by cWB [104], and sky localization was only performed on triggers also detected by BayesWave (and not classified as noise or a glitch). The median localization was shown to be $\sim 100-200$ deg^2 for a two-detector network in O1 and $\sim 60-110$ deg^2 for a three-detector network in O2, with the localization and relative performance of the algorithms depending upon the waveform morphology. Results for Gaussian, sine–Gaussian, broadband white-noise and BBH waveforms are shown in Figure 7 (for the two-detector O1 network and the three-detector O2 network, cf. Figure 6). The variety of waveform morphologies reflect the range of waveforms that could be detected in a burst search [105].

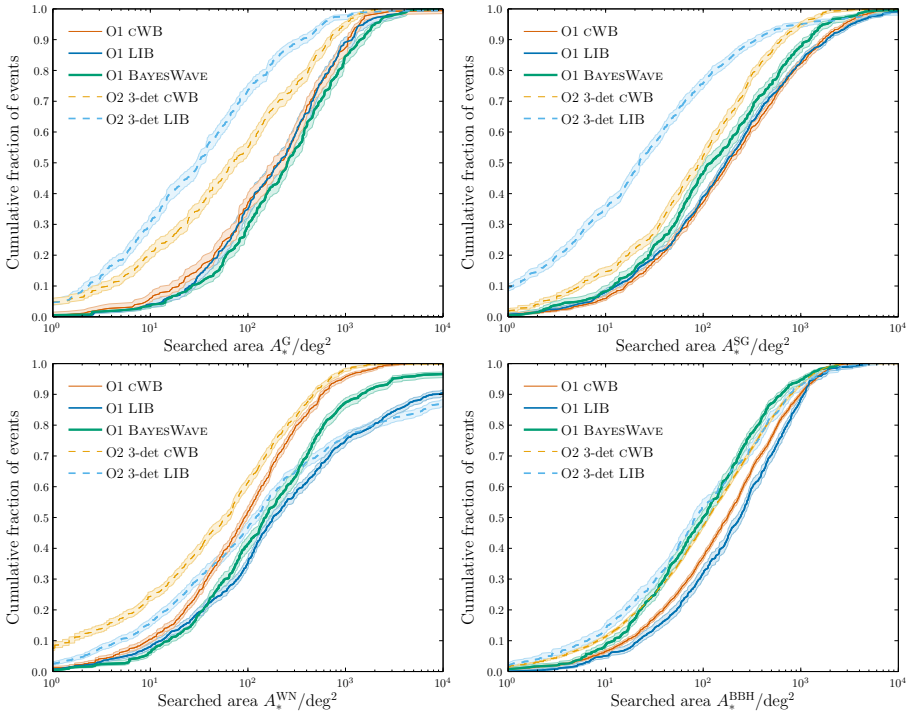

Fig. 7 Simulated sky localization for Gaussian (G; *top left*), sine–Gaussian (SG; *top right*), broadband white-noise (WN; *bottom left*) and binary black hole (BBH; *bottom right*) bursts during the first two observing runs (O1, see Section 4.1, and O2, see Section 4.2). The plots show the cumulative fractions of events with searched areas A_* smaller than the abscissa value. Results are shown for the low-latency coherent WaveBurst (cWB) [232,96,183], and higher-latency LALInferenceBurst (LIB) [188] and BayesWave [102] codes. The O2 results consider only a three-detector (3-det) network; assuming an instrument duty cycle of 70 – 75%, this would be operational 34 – 42% of the time. The BayesWave results are only for O1 and include only events that could be detected by the code. The shaded areas indicate the 68% confidence intervals on the cumulative distributions. A detection threshold of a false alarm rate of approximately 1 yr^{-1} is used for cWB and LIB, and BayesWave is run as a follow-up for cWB triggers. Results are taken from [202] and [231].

A high mass BBH, like GW150914 [8], could be detected by both burst and CBC analyses. In this case, we expect that the CBC localization, which makes use of the additional information available from constraining signals to match waveform templates, is more accurate than the burst localization (cf. [233]).

4 Observing Scenarios

In this section we estimate the sensitivity, possible number of detections, and localization capability for each of the observing runs laid out in Section 2.2. We discuss each future observing run in turn and also summarize the results in Table 3.

In the following, we estimate the expected number of BNS coalescence detections using both the lower and upper estimates on the BNS source rate density, 10^{-8} – $10^{-5}\,\mathrm{Mpc}^{-3}\,\mathrm{yr}^{-1}$ [73]. Given the detectors' noise spectral densities, the ρ_c detection threshold can be converted into the (source sky-location and orientation averaged) BNS sensitive detection range R_{BNS} [73,234]. From this, the BNS source rate density can be converted into an estimate of the number of expected detected events; this estimate carries the large error on the source rate density. Similar estimates may be made for NS–BH binaries using the fact that the NS–BH range is approximately a factor of 1.6 larger than the BNS range,[8] though the uncertainty in the NS–BH source rate density is slightly larger [73]. We assume a nominal ρ_c threshold of 12, at which the expected FAR is $\sim 10^{-2}\ \mathrm{yr}^{-1}$. However, such a stringent threshold may not be appropriate for selecting candidate triggers for electromagnetic follow-up. For example, selecting CBC candidates at thresholds corresponding to a higher background rate of 1 yr^{-1} (100 yr^{-1}) would increase the number of true signals subject to electromagnetic follow-up by about 30% (90%). The area localization for these low-threshold signals is, on average, only fractionally worse than for the high-threshold population – by approximately 20% (60%). The localization of NS–BH signals is expected to be similar to that of BNS signals.

For typical burst sources, the gravitational waveform is not well known. However, the performance of burst searches is largely independent of the detailed waveform morphology [165,202], allowing us to quote an approximate sensitive range determined by the total energy E_{GW} emitted in GWs, the central frequency f_0 of the burst, the detector noise spectrum $S(f)$, and the single-detector SNR threshold ρ_{det} [235],

$$R_{\mathrm{burst}} \simeq \left[\frac{G}{2\pi^2 c^3}\frac{E_{\mathrm{GW}}}{S(f_0) f_0^2 \rho_{\mathrm{det}}^2}\right]^{1/2}. \tag{2}$$

In this article, we quote ranges using $E_{\mathrm{GW}} = 10^{-2} M_\odot c^2$ and $f_0 = 150$ Hz; $E_{\mathrm{GW}} = 10^{-2} M_\odot c^2$ is an optimistic value for GW emission from stellar collapse (see, e.g., [214]); the uncertainty in E_{GW} means that the quoted burst ranges are more uncertain than their BNS counterparts. We use a single-detector SNR threshold of 8, corresponding to a typical network SNR of ~ 12.

The run durations discussed below are in calendar time. In O1, the H1–L1 network had a duty factor of approximately 43%. Table 2 illustrates how the up time for each detector was impacted by various activities or the environment. The two biggest non-observing categories for each detector are Locking and Environmental. Locking refers to the amount of time spent in bringing the interferometers from an uncontrolled state to their lowest noise configuration [236]. Environmental effects include earthquakes, wind and the microseism noise arising from ocean storms [175,174]. The latter two effects have seasonal variation, with the prevalence of storms being higher during the

[8] This assumes a black hole mass of $5 M_\odot$.

Table 2 Percentage of time during the first observing run that the LIGO detectors spent in different operating modes as entered by the on-duty operator. Since several factors may influence detector operation at any given time, there is a certain subjectivity to the assignments. Maintenance includes a planned 4-hour weekly period ($\sim 2.4\%$ of the total). Coincident operation of the detectors occurred $\sim 43\%$ of the time.

Detector		Hanford	Livingston
Operating mode	Observing	64.6%	57.4%
	Locking	17.9%	16.1%
	Environmental	9.7%	19.8%
	Maintenance	4.4%	4.9%
	Commissioning	2.9%	1.6%
	Planned engineering	0.1%	0.0%
	Other	0.4%	0.4%

winter months. L1 has a greater sensitivity to microseism noise and to earthquakes than H1 mainly due to the local geophysical environment [237]. During O1, L1 lost over twice as much observing time to earthquakes, microseism noise and wind than did H1. While we can expect some improvement in duty factors from operating during non-winter months, we can continue to expect at least a 10% impact on operating time from environmental effects. Adding in maintenance, both planned and unplanned, and time spent in locking we currently expect duty factors of at most 70 – 75% for each instrument during extended runs. Assuming downtime periods are uncorrelated among detectors, this means that all detectors in a three-detector network will be operating in coincidence approximately 34 – 42% of the time, and at least two detectors will be operating for 78 – 84% of the time. For a four-detector network, three or more detectors will be operational around 65 – 74% of the time, and for a five-detector network, three of more detectors will be operating for 84 – 90% of the time. Our estimates for the expected number of detections and the fraction of sources localized account for these duty cycles. The downtime periods are sometimes correlated between detectors, for example planned maintenance periods are often coordinated, and so these coincidence times may be conservative estimates. The number of detections also account for the uncertainty in the detector sensitive ranges as indicated in Figure 1, but do not include any cosmological evolution of the merger rate.

4.1 2015 – 2016 run (O1): aLIGO

This was the first advanced-detector observing run, lasting four months, starting 12 September 2015 and ending 19 January 2016.

The aLIGO sensitivity was expected to be similar to the early band in Figure 1, with a BNS range of 40 – 80 Mpc, and a burst range of 40 – 60 Mpc for $E_{\rm GW} = 10^{-2} M_{\odot} c^2$. The achieved sensitivity was at the better end of this span, with a BNS range of $\sim$ 60 – 80 Mpc.

The O1 BNS search volume was $\sim 2 \times 10^5$ Mpc^3 yr, and the dominant source of uncertainty on this value is the calibration of the detectors [68]. The search volume is $V_z T$, where $V_z = (4\pi/3) R^3$ is the time-averaged volume surveyed and T is the observing time incorporating the effects of the detectors' duty cycles. We would

therefore expect 0.002 – 2 BNS detections. No BNS detections were made, consistent with these expectations [68].

With the two-detector H1–L1 network any detected events are unlikely to be well localized. A full parameter-estimation study using realistic detector noise and an astrophysically-motivated source catalog has been completed for 2015 – 2016 [187].[9] This used a noise curve in the middle of the early range shown in Figure 1 (the early curve specified in [238]). The distribution of results is shown in Figure 6. In Table 3, we present results calculated using BAYESTAR [189] for a population of BNS signals, assuming an SNR threshold of 12; the results agree with those of [187]. The median 90% credible region for is 460 – 530 deg^2; the searched area $A_*^{\rm BNS}$ is smaller than 20 deg^2 for 14 – 17% of events and smaller than 5 deg^2 in 4 – 6%.

Equivalent (but not directly comparable) results for bursts are found in [202]. Specific results depend upon the waveform morphology used, but the median searched area is $\sim 1-2$ times larger than for BNS signals; part of this difference is due to the burst study using a less-stringent FAR threshold of ~ 1 yr^{-1}. The distribution of searched areas for four waveform morphologies are shown in Figure 7.

The localizations of GW150914, GW151226 and LVT151012 exhibit the characteristic broken arc for a two-detector network [9,18]. The 90% credible regions are 230 deg^2, 850 deg^2 and 1600 deg^2 respectively [18]. The sky localization for a CBC signal consistent with the properties of GW150914 is shown in Figure 8. This shows the localization with the two-detector O1 network as well as with other detector network configurations [229].

The poor localization from a two-detector network makes follow-up challenging. The electromagnetic follow-up effort for GW150914 is described in [9,108], and the search for coincident neutrinos is described in [10,11].

4.2 2016 – 2017 run (O2): aLIGO joined by AdV

This was an approximately nine-month run with three detectors for the second part of the run. The aLIGO performance was expected to be similar to the mid band in Figure 1, with a BNS range of 80 – 120 Mpc, and a burst range of 60 – 75 Mpc for $E_{\rm GW} = 10^{-2} M_\odot c^2$: the achieved BNS range is towards the lower part of this band, around 60 – 100 Mpc [19]. The AdV range was anticipated to be within the early band in Figure 1, approximately 20 – 65 Mpc for BNS and 20 – 40 Mpc for bursts. On 1 August 2017, AdV joined O2 with a BNS range of 25 – 30 Mpc.

The potential improvement in sky localization from the addition of a third detector is illustrated in Figure 8.

Anticipated BNS sky localization for 2016 – 2017 (in addition to 2015 – 2016) was investigated in [195]. This assumed a noise curve which lies in the middle of the mid range in Figure 1 for aLIGO (the mid curve specified in [238]) and the geometric mean of the upper and lower bounds of the mid region in Figure 1 for AdV. The distribution of results is shown in Figure 6. In Table 3, we give results for an astrophysically-motivated BNS population, with an SNR threshold of 12, assuming a three-detector

[9] This study used noise from the sixth science run of initial LIGO, recolored to the expected O1 sensitivity curve. The source catalog, as well as the analysis pipeline, is shared in [195].

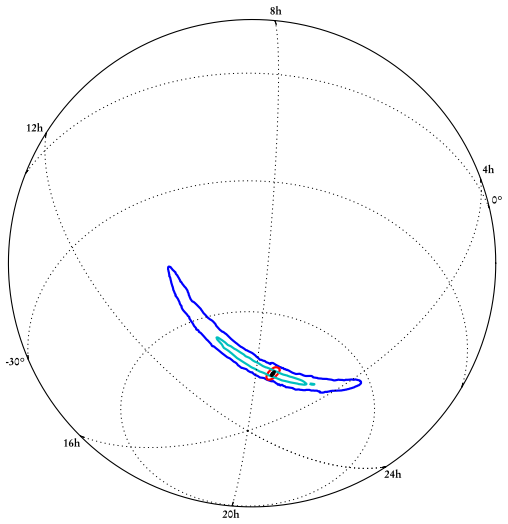

Fig. 8 Sky localization of a signal with parameters consistent with those for GW150914. The lines enclose the 90% credible regions with different detector networks. Dark blue is for the O1 two-detector network; light blue is for the same Hanford–Livingston network at design sensitivity; red is for the three-detector network including Virgo, with all detectors at early sensitivity, similar to what was expected for O2, and black is for the three detector network at design sensitivity. The plot is an orthographic projection with right ascension measured in hours and declination measured in degrees. Figure adapted from [229].

network with each detector having an individual duty cycle of 70 – 75%. The results are calculated using BAYESTAR. The median 90% credible region is 230 – 320 deg^2, and 7 – 13% of events are expected to have $\mathrm{CR}_{0.9}^{\mathrm{BNS}}$ smaller than 20 deg^2. The searched area is smaller than 20 deg^2 for 33 – 41% of events and smaller than 5 deg^2 for 16 – 21%. The burst study [202] gives approximately equivalent results, producing median searched areas a factor of $\sim 2-3$ larger than the BNS results; these results are shown in Figure 7.

4.3 2018 – 2019 run (O3): aLIGO 120 – 170 Mpc, AdV 65 – 85 Mpc

This is envisioned to be a year long run with three detectors. The aLIGO and AdV sensitivities will be similar to the late and mid bands of Figure 1 respectively, with BNS ranges of 120 – 170 Mpc and 65 – 85 Mpc, and burst ranges of 75 – 90 Mpc and 40 – 50 Mpc for $E_{\mathrm{GW}} = 10^{-2} M_{\odot} c^2$. This gives an expected 0.04 – 100 BNS detections. Both the range and the typical sky localization should increase relative to the 2016 – 2017 run. Table 3 gives BAYESTAR localizations assuming detector sensitivities which are the geometric means of the upper and lower bounds of the relevant bands in Figure 1. The median 90% credible region is 120 – 180 deg^2, and 12 – 21% of events are expected to have $\mathrm{CR}_{0.9}^{\mathrm{BNS}}$ smaller than 20 deg^2.

4.4 2020+ runs: aLIGO 190 Mpc, AdV 65 – 125 Mpc

At this point we anticipate extended runs with the detectors at or near design sensitivity. The aLIGO detectors are expected to have a sensitivity curve similar to the design curve of Figure 1. AdV may be operating similarly to the late band, eventually reaching the design sensitivity circa 2021. This gives an expected 0.1 – 200 BNS detections annually. Potential localization for a GW150914-like BBH signal is shown in Figure 8. The fraction of signals localized to areas of a few square degrees is increased compared to previous runs. This is due to the much larger detector bandwidths, particularly for AdV, as well as the increased sensitivity of the network; see Figure 1.

4.5 2024+ runs: aLIGO (including LIGO-India) 190 Mpc, AdV 125 Mpc, KAGRA 140 Mpc

The five-site network incorporating LIGO-India at design sensitivity would have both improved sensitivity and better localization capabilities. The per-year BNS search volume increases giving an expected 0.4 – 400 BNS detections annually. The addition of more detector sites leads to good source localization over the whole sky [228, 62, 63, 64]. Table 3 gives BAYESTAR localizations for an astrophysical population of BNSs, assuming design sensitivity and a 70 – 75% duty cycle for each detector. The median 90% credible region is 9 – 12 deg^2, 65 – 73% of events are expected to have $\mathrm{CR}^{\mathrm{BNS}}_{0.9}$ smaller than 20 deg^2, and the searched area is less than 20 deg^2 for 87 – 90%.

Table 3 Summary of a plausible observing schedule, expected sensitivities, and source localization with the Advanced LIGO, Advanced Virgo and KAGRA detectors, which will be strongly dependent on the detectors' commissioning progress. Ranges reflect the uncertainty in the detector noise spectra shown in Figure 1. The achieved binary neutron star (BNS) ranges for 2016 – 2017 are characteristic of performance to date, not for the complete run. The burst ranges assume standard-candle emission of $10^{-2} M_{\odot} c^2$ in gravitational waves at 150 Hz and scale as $E_{\rm GW}^{1/2}$, so it is greater for more energetic sources (such as binary black holes). The BNS localization is characterized by the size of the 90% credible region (CR) and the searched area. These are calculated by running the BAYESTAR rapid sky-localization code [189] on a Monte Carlo sample of simulated signals, assuming senisivity curves in the middle of the plausible ranges (the geometric means of the upper and lower bounds). The variation in the localization reflects both the variation in duty cycle between 70% and 75% as well as Monte Carlo statistical uncertainty. The estimated number of BNS detections uses the actual BNS for 2015 – 2016, and the expected range otherwise; future runs assume a 70 – 75% duty cycle for each instrument. The BNS detection numbers also account for the uncertainty in the BNS source rate density [73]. Estimated BNS detection numbers and localization estimates are computed assuming a signal-to-noise ratio greater than 12. Burst localizations are expected to be broadly similar to those derived from timing triangulation, but vary depending on the signal bandwidth; the median burst searched area (with a false alarm rate of ~ 1 yr^{-1}) may be a factor of $\sim 2-3$ larger than the values quoted for BNS signals [202]. No burst detection numbers are given, since the source rates are currently unknown. Numbers for 2016 – 2017 include Virgo, and do not take into account that Virgo only joined the observations for the latter part the run. The 2024+ scenario includes LIGO-India at design sensitivity.

Epoch			2015 – 2016	2016 – 2017	2018 – 2019	2020+	2024+
Planned run duration			4 months	9 months	12 months	(per year)	(per year)
Expected burst range/Mpc		LIGO	40 – 60	60 – 75	75 – 90	105	105
		Virgo	—	20 – 40	40 – 50	40 – 70	80
		KAGRA	—	—	—	—	100
Expected BNS range/Mpc		LIGO	40 – 80	80 – 120	120 – 170	190	190
		Virgo	—	20 – 65	65 – 85	65 – 115	125
		KAGRA	—	—	—	—	140
Achieved BNS range/Mpc		LIGO	60 – 80	*60 – 100*	—	—	—
		Virgo	—	*25 – 30*	—	—	—
		KAGRA	—	—	—	—	—
Estimated BNS detections			0.002 – 2	0.007 – 30	0.04 – 100	0.1 – 200	0.4 – 400
Actual BNS detections			0	—	—	—	—
90% CR	% within	5 deg^2	< 1	1 – 5	1 – 4	3 – 7	23 – 30
		20 deg^2	< 1	7 – 14	12 – 21	14 – 22	65 – 73
	median/deg^2		460 – 530	230 – 320	120 – 180	110 – 180	9 – 12
Searched area	% within	5 deg^2	4 – 6	15 – 21	20 – 26	23 – 29	62 – 67
		20 deg^2	14 – 17	33 – 41	42 – 50	44 – 52	87 – 90

5 Conclusions

We have presented possible observing scenarios for the Advanced LIGO, Advanced Virgo and KAGRA network of GW detectors, with emphasis on the expected sensitivities and sky-localization accuracies. This network began operation in September 2015. The first BBH detection was made promptly after the start of observations. However, unless the most optimistic astrophysical rates hold, two or more detectors with an average range of at least 100 Mpc and with a run of several months will be required for BNS detection.

Electromagnetic follow-up of GW candidates *may* help confirm GW candidates that would not be confidently identified from GW observations alone. However, such follow-ups need to deal with large position uncertainties, with areas of many tens to thousands of square degrees. This is likely to remain the situation until late in the decade. Optimizing the electromagnetic follow-up and source identification is an outstanding research topic (see, e.g., [106,239,240,195,181,241,242,243,244,245]). Triggering of focused searches in GW data by electromagnetically-detected events can also help in recovering otherwise hidden GW signals [215].

Sky localization is poor until a third detector reaches a sensitivity within a factor of ~ 4 of the others and with a broad frequency bandwidth [246,247]; this was achieved in the latter part of O2. With a four- or five-site detector network at final design sensitivity, we may expect a significant fraction of GW signals to be localized to within a few square degrees by GW observations alone.

The purpose of this article is to provide information to the astronomy community to facilitate planning for multi-messenger astronomy with advanced GW detectors. *While the scenarios described here are our best current projections, they will evolve as detector installation and commissioning progress.* We will therefore update this article regularly.

Acknowledgements The authors gratefully acknowledge the support of the United States National Science Foundation (NSF) for the construction and operation of the LIGO Laboratory and Advanced LIGO as well as the Science and Technology Facilities Council (STFC) of the United Kingdom, the Max-Planck-Society (MPS), and the State of Niedersachsen/Germany for support of the construction of Advanced LIGO and construction and operation of the GEO 600 detector. Additional support for Advanced LIGO was provided by the Australian Research Council. The authors gratefully acknowledge the Italian Istituto Nazionale di Fisica Nucleare (INFN), the French Centre National de la Recherche Scientifique (CNRS) and the Foundation for Fundamental Research on Matter supported by the Netherlands Organisation for Scientific Research, for the construction and operation of the Virgo detector and the creation and support of the EGO consortium. The authors also gratefully acknowledge research support from these agencies as well as by the Council of Scientific and Industrial Research of India, Department of Science and Technology, India, Science & Engineering Research Board (SERB), India, Ministry of Human Resource Development, India, the Spanish Ministerio de Economía y Competitividad, the Conselleria d'Economia i Competitivitat and Conselleria d'Educaci, Cultura i Universitats of the Govern de les Illes Balears, the National Science Centre of Poland, the FOCUS Programme of Foundation for Polish Science, the European Union, the Royal Society, the Scottish Funding Council, the Scottish Universities Physics Alliance, the Lyon Institute of Origins (LIO), the National Research Foundation of Korea, Industry Canada and the Province of Ontario through the Ministry of Economic Development and Innovation, the National Science and Engineering Research Council Canada, the Brazilian Ministry of Science, Technology, and Innovation, the Research Corporation, Ministry of Science and Technology (MOST), Taiwan and the Kavli Foundation. The authors gratefully acknowledge the support of the NSF, STFC, MPS, INFN, CNRS and the State of Niedersachsen/Germany for provision of computational resources. The authors gratefully acknowledge the support in Japan by MEXT, JSPS Leading-edge Research Infrastructure Program, JSPS Grant-in-Aid for Specially Promoted Research 26000005, MEXT Grant-in-Aid for Scientific Research on Innovative Areas 24103005, JSPS Core-to-Core Program, A. Advanced Research Networks, the joint research program of the Institute for Cosmic Ray Research, University of Tokyo, and Computing Infrastructure Project of KISTI-GSDC in Korea. This article has been assigned LIGO Document number P1200087, Virgo Document number VIR-0288A-12, and KAGRA Document number JGW-P1706792.

A Changes between versions

Since publication of the previous version [30], several updates to the document have been made. The most significant changes are the inclusion of details regarding KAGRA and results from O1. The key differences are outlined below.

A.1 Updates to detector commissioning

The plausible detector scenarios remain largely unchanged, but details of O1 and O2 have been updated. Specific updates to the detector scenarios are:

1. The addition of KAGRA to Figure 1 and Figure 2.
2. Table 1 has been added which includes BNS ranges and $30M_{\odot}$+$30M_{\odot}$ BBH ranges.
3. The O1 sensitivity has been updated following the completion of the run (12 September 2015 – 19 January 2016). We believed that the O1 BNS range would plausibly be 40 – 80 Mpc, and the actual range was 60 – 80 Mpc.
4. The formal transition to O2 was 30 November 2016 , and the run ended 25 August 2017. The run is approximately nine calendar months in duration, but includes a two-week break at the end of December and a three-week commissioning break in May. The achieved aLIGO BNS range so far was approximately 60 – 100 Mpc [19].
5. The AdV detector officially joined the O2 run on 1 August 2017. The achieved AdV BNS range was approximately 25 – 30 Mpc.
6. As a consequence of the extended O2 run, the start of O3 is now expected to be in 2018, approximately a year after the end of O2. O3 is now planned to be a year in duration.
7. Figure 2 has been updated to show the current planned timeline.
8. Based on our experience in O1 and O2, we have revised our predicted duty cycles, we believe that single-detector duty cycles of 70% – 75% for extended runs are more realistic than the previous value of 80%.
9. We have updated the final observing scenario, the 2024+ case, to be a five-detector network including KAGRA.
10. Progress has been made towards establishing LIGO-India, with the the Indian government granting in-principle approval; however, it is still too early to give a definite timeline for the observing schedule. 2024 is the earliest we imagine it could be operational.
11. Some of the BNS ranges associated with different observing scenarios have changed as a result of using an updated calculation, including cosmological corrections. For all cosmological calculations, we assume a flat cosmology with Hubble parameter $H_0 = 67.9\ \mathrm{km\,s^{-1}\,Mpc^{-1}}$, and density parameters $\Omega_{\mathrm{m}} = 0.3065$ and $\Omega_{\Lambda} = 0.6935$ [248]. The sensitivity curves themselves have not been modified. Ranges are rounded to the nearest megaparsec below 15 Mpc, rounded to the nearest 5 Mpc between 15 Mpc and 1000 Mpc, and to the nearest 10 Mpc above 1000 Mpc.

A.2 Updates to data analysis

In addition to the progress made with regards to the detectors, there have also been significant advances from analysing the data. We now include results from O1 [18,68,67]; these include the first detections, which correspond to BBH systems [8,17,18]. Multi-messenger searches for counterparts to these detections are described in [9,108,10,11]. Specific updates that have been made are:

1. Figure 3 has been updated to include O1 results; the surrounding text has been updated to discuss the detection pipelines used in O1 [65,18,66,67].
2. Results using the BAYESWAVE algorithm [231], appropriate for O1, have been included in Figure 7.
3. Figure 8 shows a sky localization, created using current parameter-estimation techniques, illustrating how localization improves for different network configurations for a GW150914-like signal [229].
4. Table 3 now includes numbers summarising results from O1 and the new 2024+ scenario including KAGRA. Sky localization numbers for are now calculated using BAYESTAR [189] for all epochs.

While the first detection of O2 (a new BBH system) has been announced [19], we defer describing the full results of this run until a future update.

B Author list

B. P. Abbott,[1] R. Abbott,[1] T. D. Abbott,[2] M. R. Abernathy,[3] F. Acernese,[4,5] K. Ackley,[6] C. Adams,[7] T. Adams,[8] P. Addesso,[9] R. X. Adhikari,[1] V. B. Adya,[10] C. Affeldt,[10] M. Agathos,[11] K. Agatsuma,[11] N. Aggarwal,[12] O. D. Aguiar,[13] L. Aiello,[14,15] A. Ain,[16] P. Ajith,[17] T. Akutsu,[18] B. Allen,[10,19,20] A. Allocca,[21,22] P. A. Altin,[23] A. Ananyeva,[1] S. B. Anderson,[1] W. G. Anderson,[19] M. Ando,[24,18,25] S. Appert,[1] K. Arai,[1] A. Araya,[26] M. C. Araya,[1] J. S. Areeda,[27] N. Arnaud,[28] K. G. Arun,[29] H. Asada,[30] S. Ascenzi,[31,15] G. Ashton,[10] Y. Aso,[18] M. Ast,[32] S. M. Aston,[7] P. Astone,[33] S. Atsuta,[34] P. Aufmuth,[20] C. Aulbert,[10] A. Avila-Alvarez,[27] K. Awai,[35] S. Babak,[36] P. Bacon,[37] M. K. M. Bader,[11] L. Baiotti,[38] P. T. Baker,[39,40] F. Baldaccini,[41,42] G. Ballardin,[43] S. W. Ballmer,[44] J. C. Barayoga,[1] S. E. Barclay,[45] B. C. Barish,[1] D. Barker,[46] F. Barone,[4,5] B. Barr,[45] L. Barsotti,[12] M. Barsuglia,[37] D. Barta,[47] J. Bartlett,[46] M.A. Barton,[18] I. Bartos,[48] R. Bassiri,[49] A. Basti,[21,22] J. C. Batch,[46] C. Baune,[10] V. Bavigadda,[43] M. Bazzan,[50,51] B. Bécsy,[52] C. Beer,[10] M. Bejger,[53] I. Belahcene,[28] M. Belgin,[54] A. S. Bell,[45] B. K. Berger,[1] G. Bergmann,[10] C. P. L. Berry,[55] D. Bersanetti,[56,57] A. Bertolini,[11] J. Betzwieser,[7] S. Bhagwat,[44] R. Bhandare,[58] I. A. Bilenko,[59] G. Billingsley,[1] C. R. Billman,[6] J. Birch,[7] R. Birney,[60] O. Birnholtz,[10] S. Biscans,[12,1] A. Bisht,[20] M. Bitossi,[43] C. Biwer,[44] M. A. Bizouard,[28] J. K. Blackburn,[1] J. Blackman,[61] C. D. Blair,[62] D. G. Blair,[62] R. M. Blair,[46] S. Bloemen,[63] O. Bock,[10] M. Boer,[64] G. Bogaert,[64] A. Bohe,[36] F. Bondu,[65] R. Bonnand,[8] B. A. Boom,[11] R. Bork,[1] V. Boschi,[21,22] S. Bose,[66,16] Y. Bouffanais,[37] A. Bozzi,[43] C. Bradaschia,[22] P. R. Brady,[19] V. B. Braginsky*,[59] M. Branchesi,[67,68] J. E. Brau,[69] T. Briant,[70] A. Brillet,[64] M. Brinkmann,[10] V. Brisson,[28] P. Brockill,[19] J. E. Broida,[71] A. F. Brooks,[1] D. A. Brown,[44] D. D. Brown,[55] N. M. Brown,[12] S. Brunett,[1] C. C. Buchanan,[2] A. Buikema,[12] T. Bulik,[72] H. J. Bulten,[73,11] A. Buonanno,[36,74] D. Buskulic,[8] C. Buy,[37] R. L. Byer,[49] M. Cabero,[10] L. Cadonati,[54] G. Cagnoli,[75,76] C. Cahillane,[1] J. Calderón Bustillo,[54] T. A. Callister,[1] E. Calloni,[77,5] J. B. Camp,[78] K. C. Cannon,[25] H. Cao,[79] J. Cao,[80] C. D. Capano,[10] E. Capocasa,[37] F. Carbognani,[43] S. Caride,[81] J. Casanueva Diaz,[28] C. Casentini,[31,15] S. Caudill,[19] M. Cavaglià,[82] F. Cavalier,[28] R. Cavalieri,[43] G. Cella,[22] C. B. Cepeda,[1] L. Cerboni Baiardi,[67,68] G. Cerretani,[21,22] E. Cesarini,[31,15] S. J. Chamberlin,[83] M. Chan,[45] S. Chao,[84] P. Charlton,[85] E. Chassande-Mottin,[37] B. D. Cheeseboro,[39,40] H. Y. Chen,[86] Y. Chen,[61] H.-P. Cheng,[6] A. Chincarini,[57] A. Chiummo,[43] T. Chmiel,[87] H. S. Cho,[88] M. Cho,[74] J. H. Chow,[23] N. Christensen,[71] Q. Chu,[62] A. J. K. Chua,[89] S. Chua,[70] S. Chung,[62] G. Ciani,[6] F. Clara,[46] J. A. Clark,[54] F. Cleva,[64] C. Cocchieri,[82] E. Coccia,[14,15] P.-F. Cohadon,[70] A. Colla,[90,33] C. G. Collette,[91] L. Cominsky,[92] M. Constancio Jr.,[13] L. Conti,[51] S. J. Cooper,[55] T. R. Corbitt,[2] N. Cornish,[93] A. Corsi,[81] S. Cortese,[43] C. A. Costa,[13] M. W. Coughlin,[71] S. B. Coughlin,[94] J.-P. Coulon,[64] S. T. Countryman,[48] P. Couvares,[1] P. B. Covas,[95] E. E. Cowan,[54] D. M. Coward,[62] M. J. Cowart,[7] D. C. Coyne,[1] R. Coyne,[81] J. D. E. Creighton,[19] T. D. Creighton,[96] J. Cripe,[2] S. G. Crowder,[97] T. J. Cullen,[27] A. Cumming,[45] L. Cunningham,[45] E. Cuoco,[43] T. Dal Canton,[78] S. L. Danilishin,[45] S. D'Antonio,[15] K. Danzmann,[20,10] A. Dasgupta,[98] C. F. Da Silva Costa,[6] V. Dattilo,[43] I. Dave,[58] M. Davier,[28] G. S. Davies,[45] D. Davis,[44] E. J. Daw,[99] B. Day,[54] R. Day,[43] S. De,[44] D. DeBra,[49] G. Debreczeni,[47] J. Degallaix,[75] M. De Laurentis,[77,5] S. Deléglise,[70] W. Del Pozzo,[55] T. Denker,[10] T. Dent,[10] V. Dergachev,[36] R. De Rosa,[77,5] R. T. DeRosa,[7] R. DeSalvo,[100,9] R. C. Devine,[39,40] S. Dhurandhar,[16] M. C. Díaz,[96] L. Di Fiore,[5] M. Di Giovanni,[101,102] T. Di Girolamo,[77,5] A. Di Lieto,[21,22] S. Di Pace,[90,33] I. Di Palma,[36,90,33] A. Di Virgilio,[22] Z. Doctor,[86] K. Doi,[103] V. Dolique,[75] F. Donovan,[12] K. L. Dooley,[82] S. Doravari,[10] I. Dorrington,[104] R. Douglas,[45] M. Dovale Álvarez,[55] T. P. Downes,[19] M. Drago,[10] R. W. P. Drever†,[1] J. C. Driggers,[46] Z. Du,[80] M. Ducrot,[8] S. E. Dwyer,[46] K. Eda,[25] T. B. Edo,[99] M. C. Edwards,[71] A. Effler,[7] H.-B. Eggenstein,[10] P. Ehrens,[1] J. Eichholz,[1] S. S. Eikenberry,[6] R. A. Eisenstein,[12] R. C. Essick,[12] Z. Etienne,[39,40] T. Etzel,[1] M. Evans,[12] T. M. Evans,[7] R. Everett,[83] M. Factourovich,[48] V. Fafone,[31,15,14] H. Fair,[44] S. Fairhurst,[104] X. Fan,[80] S. Farinon,[57] B. Farr,[86] W. M. Farr,[55] E. J. Fauchon-Jones,[104] M. Favata,[105] M. Fays,[104] H. Fehrmann,[10] M. M. Fejer,[49] A. Fernández Galiana,[12] I. Ferrante,[21,22] E. C. Ferreira,[13] F. Ferrini,[43] F. Fidecaro,[21,22] I. Fiori,[43] D. Fiorucci,[37] R. P. Fisher,[44] R. Flaminio,[75,18] M. Fletcher,[45] H. Fong,[106] S. S. Forsyth,[54] J.-D. Fournier,[64] S. Frasca,[90,33] F. Frasconi,[22] Z. Frei,[52] A. Freise,[55] R. Frey,[69] V. Frey,[28] E. M. Fries,[1] P. Fritschel,[12] V. V. Frolov,[7] Y. Fujii,[18] M.-K. Fujimoto,[18] P. Fulda,[6,78] M. Fyffe,[7] H. Gabbard,[10] B. U. Gadre,[16] S. M. Gaebel,[55] J. R. Gair,[107] L. Gammaitoni,[41] S. G. Gaonkar,[16] F. Garufi,[77,5] G. Gaur,[108] V. Gayathri,[109] N. Gehrels†,[78] G. Gemme,[57] E. Genin,[43] A. Gennai,[22] J. George,[58] L. Gergely,[110] V. Germain,[8] S. Ghonge,[17] Abhirup Ghosh,[17] Archisman Ghosh,[11,17] S. Ghosh,[63,11] J. A. Giaime,[2,7] K. D. Giardina,[7] A. Giazotto,[22] K. Gill,[111] A. Glaefke,[45] E. Goetz,[10] R. Goetz,[6] L. Gondan,[52] G. González,[2] J. M. Gonzalez Castro,[21,22] A. Gopakumar,[112] M. L. Gorodetsky,[59] S. E. Gossan,[1] M. Gosselin,[43] R. Gouaty,[8] A. Grado,[113,5] C. Graef,[45] M. Granata,[75] A. Grant,[45] S. Gras,[12] C. Gray,[46] G. Greco,[67,68] A. C. Green,[55] P. Groot,[63] H. Grote,[10] S. Grunewald,[36] G. M. Guidi,[67,68] X. Guo,[80] A. Gupta,[16] M. K. Gupta,[98] K. E. Gushwa,[1] E. K. Gustafson,[1] R. Gustafson,[114] J. J. Hacker,[27] A. Hagiwara,[115] B. R. Hall,[66] E. D. Hall,[1] G. Hammond,[45] M. Haney,[112]

M. M. Hanke,[10] J. Hanks,[46] C. Hanna,[83] M. D. Hannam,[104] J. Hanson,[7] T. Hardwick,[2] J. Harms,[67,68] G. M. Harry,[3] I. W. Harry,[36] M. J. Hart,[45] M. T. Hartman,[6] C.-J. Haster,[55,106] K. Haughian,[45] K. Hayama,[35] J. Healy,[116] A. Heidmann,[70] M. C. Heintze,[7] H. Heitmann,[64] P. Hello,[28] G. Hemming,[43] M. Hendry,[45] I. S. Heng,[45] J. Hennig,[45] J. Henry,[116] A. W. Heptonstall,[1] M. Heurs,[10,20] S. Hild,[45] E. Hirose,[35] D. Hoak,[43] D. Hofman,[75] K. Holt,[7] D. E. Holz,[86] P. Hopkins,[104] J. Hough,[45] E. A. Houston,[45] E. J. Howell,[62] Y. M. Hu,[10] E. A. Huerta,[117] D. Huet,[28] B. Hughey,[111] S. Husa,[95] S. H. Huttner,[45] T. Huynh-Dinh,[7] N. Indik,[10] D. R. Ingram,[46] R. Inta,[81] K. Ioka,[118] H. N. Isa,[45] J.-M. Isac,[70] M. Isi,[1] T. Isogai,[12] Y. Itoh,[25] B. R. Iyer,[17] K. Izumi,[46] T. Jacqmin,[70] K. Jani,[54] P. Jaranowski,[119] S. Jawahar,[120] F. Jiménez-Forteza,[95] W. W. Johnson,[2] D. I. Jones,[121] R. Jones,[45] R. J. G. Jonker,[11] L. Ju,[62] J. Junker,[10] T. Kagawa,[103] T. Kajita,[35] M. Kakizaki,[103] C. V. Kalaghatgi,[104] V. Kalogera,[94] M. Kamiizumi,[35] N. Kanda,[122] S. Kandhasamy,[82] S. Kanemura,[103] M. Kaneyama,[122] G. Kang,[88] J. B. Kanner,[1] S. Karki,[69] K. S. Karvinen,[10] M. Kasprzack,[2] Y. Kataoka,[34] E. Katsavounidis,[12] W. Katzman,[7] S. Kaufer,[20] T. Kaur,[62] K. Kawabe,[46] N. Kawai,[34] S. Kawamura,[35] F. Kéfélian,[64] D. Keitel,[95] D. B. Kelley,[44] R. Kennedy,[99] J. S. Key,[123] F. Y. Khalili,[59] I. Khan,[14] S. Khan,[104] Z. Khan,[98] E. A. Khazanov,[124] N. Kijbunchoo,[46] C. Kim,[125] H. Kim,[126] J. C. Kim,[127] J. Kim,[128] W. Kim,[79] Y.-M. Kim,[129,130] S. J. Kimbrell,[54] N. Kimura,[115] E. J. King,[79] P. J. King,[46] R. Kirchhoff,[10] J. S. Kissel,[46] B. Klein,[94] L. Kleybolte,[32] S. Klimenko,[6] P. Koch,[10] S. M. Koehlenbeck,[10] Y. Kojima,[131] K. Kokeyama,[35] S. Koley,[11] K. Komori,[24] V. Kondrashov,[1] A. Kontos,[12] M. Korobko,[32] W. Z. Korth,[1] K. Kotake,[132] I. Kowalska,[72] D. B. Kozak,[1] C. Krämer,[10] V. Kringel,[10] B. Krishnan,[10] A. Królak,[133,134] G. Kuehn,[10] P. Kumar,[106] Rahul Kumar,[115] Rakesh Kumar,[98] L. Kuo,[84] K. Kuroda,[35] A. Kutynia,[133] Y. Kuwahara,[24] B. D. Lackey,[36,44] M. Landry,[46] R. N. Lang,[19] J. Lange,[116] B. Lantz,[49] R. K. Lanza,[12] A. Lartaux-Vollard,[28] P. D. Lasky,[135] M. Laxen,[7] A. Lazzarini,[1] C. Lazzaro,[51] P. Leaci,[90,33] S. Leavey,[45] E. O. Lebigot,[37] C. H. Lee,[129] H. K. Lee,[136] H. M. Lee,[130] H. W. Lee,[127] K. Lee,[45] J. Lehmann,[10] A. Lenon,[39,40] M. Leonardi,[101,102] J. R. Leong,[10] N. Leroy,[28] N. Letendre,[8] Y. Levin,[135] T. G. F. Li,[137] A. Libson,[12] T. B. Littenberg,[138] J. Liu,[62] N. A. Lockerbie,[120] A. L. Lombardi,[54] L. T. London,[104] J. E. Lord,[44] M. Lorenzini,[14,15] V. Loriette,[139] M. Lormand,[7] G. Losurdo,[22] J. D. Lough,[10,20] C. O. Lousto,[116] G. Lovelace,[27] H. Lück,[20,10] A. P. Lundgren,[10] R. Lynch,[12] Y. Ma,[61] S. Macfoy,[60] B. Machenschalk,[10] M. MacInnis,[12] D. M. Macleod,[2] F. Magaña-Sandoval,[44] E. Majorana,[33] I. Maksimovic,[139] V. Malvezzi,[31,15] N. Man,[64] V. Mandic,[140] V. Mangano,[45] S. Mano,[141] G. L. Mansell,[23] M. Manske,[19] M. Mantovani,[43] F. Marchesoni,[142,42] M. Marchio,[18] F. Marion,[8] S. Márka,[48] Z. Márka,[48] A. S. Markosyan,[49] E. Maros,[1] F. Martelli,[67,68] L. Martellini,[64] I. W. Martin,[45] D. V. Martynov,[12] K. Mason,[12] A. Masserot,[8] T. J. Massinger,[1] M. Masso-Reid,[45] S. Mastrogiovanni,[90,33] F. Matichard,[12,1] L. Matone,[48] N. Matsumoto,[143] F. Matsushima,[103] N. Mavalvala,[12] N. Mazumder,[66] R. McCarthy,[46] D. E. McClelland,[23] S. McCormick,[7] C. McGrath,[19] S. C. McGuire,[144] G. McIntyre,[1] J. McIver,[1] D. J. McManus,[23] T. McRae,[23] S. T. McWilliams,[39,40] D. Meacher,[64,83] G. D. Meadors,[36,10] J. Meidam,[11] A. Melatos,[145] G. Mendell,[46] D. Mendoza-Gandara,[10] R. A. Mercer,[19] E. L. Merilh,[46] M. Merzougui,[64] S. Meshkov,[1] C. Messenger,[45] C. Messick,[83] R. Metzdorff,[70] P. M. Meyers,[140] F. Mezzani,[33,90] H. Miao,[55] C. Michel,[75] Y. Michimura,[24] H. Middleton,[55] E. E. Mikhailov,[146] L. Milano,[77,5] A. L. Miller,[6,90,33] A. Miller,[94] B. B. Miller,[94] J. Miller,[12] M. Millhouse,[93] Y. Minenkov,[15] J. Ming,[36] S. Mirshekari,[147] C. Mishra,[17] V. P. Mitrofanov,[59] G. Mitselmakher,[6] R. Mittleman,[12] O. Miyakawa,[35] A. Miyamoto,[122] T. Miyamoto,[35] S. Miyoki,[35] A. Moggi,[22] M. Mohan,[43] S. R. P. Mohapatra,[12] M. Montani,[67,68] B. C. Moore,[105] C. J. Moore,[89] D. Moraru,[46] G. Moreno,[46] W. Morii,[148] S. Morisaki,[25] Y. Moriwaki,[103] S. R. Morriss,[96] B. Mours,[8] C. M. Mow-Lowry,[55] G. Mueller,[6] A. W. Muir,[104] Arunava Mukherjee,[17] D. Mukherjee,[19] S. Mukherjee,[96] N. Mukund,[16] A. Mullavey,[7] J. Munch,[79] E. A. M. Muniz,[27] P. G. Murray,[45] A. Mytidis,[6] S. Nagano,[149] K. Nakamura,[18] T. Nakamura,[150] H. Nakano,[150] Masaya Nakano,[103] Masayuki Nakano,[35] K. Nakao,[122] K. Napier,[54] I. Nardecchia,[31,15] T. Narikawa,[122] L. Naticchioni,[90,33] G. Nelemans,[63,11] T. J. N. Nelson,[7] M. Neri,[56,57] M. Nery,[10] A. Neunzert,[114] J. M. Newport,[3] G. Newton‡,[45] T. T. Nguyen,[23] W.-T. Ni,[151,152] A. B. Nielsen,[10] S. Nissanke,[63,11] A. Nitz,[10] A. Noack,[10] F. Nocera,[43] D. Nolting,[7] M. E. N. Normandin,[96] L. K. Nuttall,[44] J. Oberling,[46] E. Ochsner,[19] E. Oelker,[12] G. H. Ogin,[153] J. J. Oh,[126] S. H. Oh,[126] M. Ohashi,[35] N. Ohishi,[18] M. Ohkawa,[154] F. Ohme,[104,10] K. Okutomi,[155] M. Oliver,[95] K. Ono,[35] Y. Ono,[103] K. Oohara,[156] P. Oppermann,[10] Richard J. Oram,[7] B. O'Reilly,[7] R. O'Shaughnessy,[116] D. J. Ottaway,[79] H. Overmier,[7] B. J. Owen,[81] A. E. Pace,[83] J. Page,[138] A. Pai,[109] S. A. Pai,[58] J. R. Palamos,[69] O. Palashov,[124] C. Palomba,[33] A. Pal-Singh,[32] H. Pan,[84] C. Pankow,[94] F. Pannarale,[104] B. C. Pant,[58] F. Paoletti,[43,22] A. Paoli,[43] M. A. Papa,[36,19,10] H. R. Paris,[49] W. Parker,[7] D. Pascucci,[45] A. Pasqualetti,[43] R. Passaquieti,[21,22] D. Passuello,[22] B. Patricelli,[21,22] B. L. Pearlstone,[45] M. Pedraza,[1] R. Pedurand,[75,157] L. Pekowsky,[44] A. Pele,[7] F.E. Peña Arellano,[18] S. Penn,[158] C. J. Perez,[46] A. Perreca,[1] L. M. Perri,[94] H. P. Pfeiffer,[106] M. Phelps,[45] O. J. Piccinni,[90,33] M. Pichot,[64] F. Piergiovanni,[67,68] V. Pierro,[9] G. Pillant,[43] L. Pinard,[75] I. M. Pinto,[9] M. Pitkin,[45] M. Poe,[19] R. Poggiani,[21,22] P. Popolizio,[43] A. Post,[10] J. Powell,[45] J. Prasad,[16] J. W. W. Pratt,[111] V. Predoi,[104] T. Prestegard,[140,19] M. Prijatelj,[10,43] M. Principe,[9] S. Privitera,[36] G. A. Prodi,[101,102] L. G. Prokhorov,[59] O. Puncken,[10] M. Punturo,[42] P. Puppo,[33] M. Pürrer,[36] H. Qi,[19]

J. Qin,[62] S. Qiu,[135] V. Quetschke,[96] E. A. Quintero,[1] R. Quitzow-James,[69] F. J. Raab,[46] D. S. Rabeling,[23] H. Radkins,[46] P. Raffai,[52] S. Raja,[58] C. Rajan,[58] M. Rakhmanov,[96] P. Rapagnani,[90,33] V. Raymond,[36] M. Razzano,[21,22] V. Re,[31] J. Read,[27] T. Regimbau,[64] L. Rei,[57] S. Reid,[60] D. H. Reitze,[1,6] H. Rew,[146] S. D. Reyes,[44] E. Rhoades,[111] F. Ricci,[90,33] K. Riles,[114] M. Rizzo,[116] N. A. Robertson,[1,45] R. Robie,[45] F. Robinet,[28] A. Rocchi,[15] L. Rolland,[8] J. G. Rollins,[1] V. J. Roma,[69] R. Romano,[4,5] J. H. Romie,[7] D. Rosińska,[159,53] S. Rowan,[45] A. Rüdiger,[10] P. Ruggi,[43] K. Ryan,[46] S. Sachdev,[1] T. Sadecki,[46] L. Sadeghian,[19] N. Sago,[160] M. Saijo,[161] Y. Saito,[35] K. Sakai,[162] M. Sakellariadou,[163] L. Salconi,[43] M. Saleem,[109] F. Salemi,[10] A. Samajdar,[164] L. Sammut,[135] L. M. Sampson,[94] E. J. Sanchez,[1] V. Sandberg,[46] J. R. Sanders,[44] Y. Sasaki,[165] B. Sassolas,[75] B. S. Sathyaprakash,[83,104] S. Sato,[166] T. Sato,[154] P. R. Saulson,[44] O. Sauter,[114] R. L. Savage,[46] A. Sawadsky,[20] P. Schale,[69] J. Scheuer,[94] E. Schmidt,[111] J. Schmidt,[10] P. Schmidt,[1,61] R. Schnabel,[32] R. M. S. Schofield,[69] A. Schönbeck,[32] E. Schreiber,[10] D. Schuette,[10,20] B. F. Schutz,[104,36] S. G. Schwalbe,[111] J. Scott,[45] S. M. Scott,[23] T. Sekiguchi,[35] Y. Sekiguchi,[167] D. Sellers,[7] A. S. Sengupta,[168] D. Sentenac,[43] V. Sequino,[31,15] A. Sergeev,[124] Y. Setyawati,[63,11] D. A. Shaddock,[23] T. J. Shaffer,[46] M. S. Shahriar,[94] B. Shapiro,[49] P. Shawhan,[74] A. Sheperd,[19] M. Shibata,[118] Y. Shikano,[169,170] T. Shimoda,[24] A. Shoda,[18] D. H. Shoemaker,[12] D. M. Shoemaker,[54] K. Siellez,[54] X. Siemens,[19] M. Sieniawska,[53] D. Sigg,[46] A. D. Silva,[13] A. Singer,[1] L. P. Singer,[78] A. Singh,[36,10,20] R. Singh,[2] A. Singhal,[14] A. M. Sintes,[95] B. J. J. Slagmolen,[23] B. Smith,[7] J. R. Smith,[27] R. J. E. Smith,[1] K. Somiya,[34] E. J. Son,[126] B. Sorazu,[45] F. Sorrentino,[57] T. Souradeep,[16] A. P. Spencer,[45] A. K. Srivastava,[98] A. Staley,[48] M. Steinke,[10] J. Steinlechner,[45] S. Steinlechner,[32,45] D. Steinmeyer,[10,20] B. C. Stephens,[19] S. P. Stevenson,[55] R. Stone,[96] K. A. Strain,[45] N. Straniero,[75] G. Stratta,[67,68] S. E. Strigin,[59] R. Sturani,[147] A. L. Stuver,[7] Y. Sugimoto,[103] T. Z. Summerscales,[171] L. Sun,[145] S. Sunil,[98] P. J. Sutton,[104] T. Suzuki,[115] B. L. Swinkels,[43] M. J. Szczepańczyk,[111] M. Tacca,[37] H. Tagoshi,[122] S. Takada,[172] H. Takahashi,[165] R. Takahashi,[18] A. Takamori,[26] D. Talukder,[69] H. Tanaka,[35] K. Tanaka,[122] T. Tanaka,[150] D. B. Tanner,[6] M. Tápai,[110] A. Taracchini,[36] D. Tatsumi,[18] R. Taylor,[1] S. Telada,[173] T. Theeg,[10] E. G. Thomas,[55] M. Thomas,[7] P. Thomas,[46] K. A. Thorne,[7] E. Thrane,[135] T. Tippens,[54] S. Tiwari,[14,102] V. Tiwari,[104] K. V. Tokmakov,[120] K. Toland,[45] T. Tomaru,[115] C. Tomlinson,[99] M. Tonelli,[21,22] Z. Tornasi,[45] C. I. Torrie,[1] D. Töyrä,[55] F. Travasso,[41,42] G. Traylor,[7] D. Trifirò,[82] J. Trinastic,[6] M. C. Tringali,[101,102] L. Trozzo,[174,22] M. Tse,[12] R. Tso,[1] K. Tsubono,[24] T. Tsuzuki,[18] M. Turconi,[64] D. Tuyenbayev,[96] T. Uchiyama,[35] T. Uehara,[175,6] S. Ueki,[165] K. Ueno,[19] D. Ugolini,[176] C. S. Unnikrishnan,[112] A. L. Urban,[1] T. Ushiba,[24] S. A. Usman,[104] H. Vahlbruch,[20] G. Vajente,[1] G. Valdes,[96] N. van Bakel,[11] M. van Beuzekom,[11] J. F. J. van den Brand,[73,11] C. Van Den Broeck,[11] D. C. Vander-Hyde,[44] L. van der Schaaf,[11] J. V. van Heijningen,[11] M.H.P.M. van Putten,[177] A. A. van Veggel,[45] M. Vardaro,[50,51] V. Varma,[61] S. Vass,[1] M. Vasúth,[47] A. Vecchio,[55] G. Vedovato,[51] J. Veitch,[55] P. J. Veitch,[79] K. Venkateswara,[178] G. Venugopalan,[1] D. Verkindt,[8] F. Vetrano,[67,68] A. Viceré,[67,68] A. D. Viets,[19] S. Vinciguerra,[55] D. J. Vine,[60] J.-Y. Vinet,[64] S. Vitale,[12] T. Vo,[44] H. Vocca,[41,42] C. Vorvick,[46] D. V. Voss,[6] W. D. Vousden,[55] S. P. Vyatchanin,[59] A. R. Wade,[1] L. E. Wade,[87] M. Wade,[87] T. Wakamatsu,[156] M. Walker,[2] L. Wallace,[1] S. Walsh,[36,10] G. Wang,[14,68] H. Wang,[55] M. Wang,[55] Y. Wang,[62] R. L. Ward,[23] J. Warner,[46] M. Was,[8] J. Watchi,[91] B. Weaver,[46] L.-W. Wei,[64] M. Weinert,[10] A. J. Weinstein,[1] R. Weiss,[12] L. Wen,[62] P. Weßels,[10] T. Westphal,[10] K. Wette,[10] J. T. Whelan,[116] B. F. Whiting,[6] C. Whittle,[135] D. Williams,[45] R. D. Williams,[1] A. R. Williamson,[104] J. L. Willis,[179] B. Willke,[20,10] M. H. Wimmer,[10,20] W. Winkler,[10] C. C. Wipf,[1] H. Wittel,[10,20] G. Woan,[45] J. Woehler,[10] J. Worden,[46] J. L. Wright,[45] D. S. Wu,[10] G. Wu,[7] W. Yam,[12] H. Yamamoto,[1] K. Yamamoto,[35] T. Yamamoto,[35] C. C. Yancey,[74] K. Yano,[34] M. J. Yap,[23] J. Yokoyama,[25] T. Yokozawa,[122] T.H. Yoon,[180] Hang Yu,[12] Haocun Yu,[12] H. Yuzurihara,[122] M. Yvert,[8] A. Zadrożny,[133] L. Zangrando,[51] M. Zanolin,[111] S. Zeidler,[18] J.-P. Zendri,[51] M. Zevin,[94] L. Zhang,[1] M. Zhang,[146] T. Zhang,[45] Y. Zhang,[116] C. Zhao,[62] M. Zhou,[94] Z. Zhou,[94] S. J. Zhu,[36,10] X. J. Zhu,[62] M. E. Zucker,[1,12] and J. Zweizig[1]

(KAGRA Collaboration, LIGO Scientific Collaboration, and Virgo Collaboration)

*Deceased, March 2016. ♯Deceased, March 2017. †Deceased, February 2017. ‡Deceased, December 2016.

[1]LIGO, California Institute of Technology, Pasadena, CA 91125, USA
[2]Louisiana State University, Baton Rouge, LA 70803, USA
[3]American University, Washington, D.C. 20016, USA
[4]Università di Salerno, Fisciano, I-84084 Salerno, Italy
[5]INFN, Sezione di Napoli, Complesso Universitario di Monte S.Angelo, I-80126 Napoli, Italy
[6]University of Florida, Gainesville, FL 32611, USA
[7]LIGO Livingston Observatory, Livingston, LA 70754, USA
[8]Laboratoire d'Annecy-le-Vieux de Physique des Particules (LAPP), Université Savoie Mont Blanc, CNRS/IN2P3, F-74941 Annecy-le-Vieux, France

[9]University of Sannio at Benevento, I-82100 Benevento, Italy and INFN, Sezione di Napoli, I-80100 Napoli, Italy
[10]Albert-Einstein-Institut, Max-Planck-Institut für Gravitationsphysik, D-30167 Hannover, Germany
[11]Nikhef, Science Park, 1098 XG Amsterdam, The Netherlands
[12]LIGO, Massachusetts Institute of Technology, Cambridge, MA 02139, USA
[13]Instituto Nacional de Pesquisas Espaciais, 12227-010 São José dos Campos, São Paulo, Brazil
[14]INFN, Gran Sasso Science Institute, I-67100 L'Aquila, Italy
[15]INFN, Sezione di Roma Tor Vergata, I-00133 Roma, Italy
[16]Inter-University Centre for Astronomy and Astrophysics, Pune 411007, India
[17]International Centre for Theoretical Sciences, Tata Institute of Fundamental Research, Bengaluru 560089, India
[18]National Astronomical Observatory of Japan, 2-21-1, Ohsawa, Mitaka-shi, Tokyo, 181-8588, Japan
[19]University of Wisconsin-Milwaukee, Milwaukee, Wisconsin 53201, USA
[20]Leibniz Universität Hannover, D-30167 Hannover, Germany
[21]Università di Pisa, I-56127 Pisa, Italy
[22]INFN, Sezione di Pisa, I-56127 Pisa, Italy
[23]Australian National University, Canberra, Australian Capital Territory 0200, Australia
[24]The University of Tokyo, Department of Physics, 7-3-1, Hongo, Bunkyo-ku, Tokyo, 113-0033, Japan
[25]The University of Tokyo, Research Center for the Early Universe, 7-3-1, Hongo, Bunkyo-ku, Tokyo, 113-0033, Japan
[26]The University of Tokyo, Earthquake Research Institute, 1-1-1, Yayoi, Bunkyo-ku, Tokyo, 113-0032, Japan
[27]California State University Fullerton, Fullerton, CA 92831, USA
[28]LAL, Univ. Paris-Sud, CNRS/IN2P3, Université Paris-Saclay, F-91898 Orsay, France
[29]Chennai Mathematical Institute, Chennai 603103, India
[30]Hirosaki University, Department of Advanced Physics, 3, Bunkyo-cho, Hirosaki-shi, Aomori, 036-8561, Japan
[31]Università di Roma Tor Vergata, I-00133 Roma, Italy
[32]Universität Hamburg, D-22761 Hamburg, Germany
[33]INFN, Sezione di Roma, I-00185 Roma, Italy
[34]Tokyo Institute of Technology, Graduate School of Science and Technology, 2-12-1, Ookayama, Meguro-ku, Tokyo, 152-8551, Japan
[35]The University of Tokyo, Institute for Cosmic Ray Research, Higashi-Mozumi 238, Kamioka-cho, Hida-shi, Gifu 506-1205, Japan
[36]Albert-Einstein-Institut, Max-Planck-Institut für Gravitationsphysik, D-14476 Potsdam-Golm, Germany
[37]APC, AstroParticule et Cosmologie, Université Paris Diderot, CNRS/IN2P3, CEA/Irfu, Observatoire de Paris, Sorbonne Paris Cité, F-75205 Paris Cedex 13, France
[38]Osaka University, Graduate School of Science, Physics, 1-1, Machikaneyama-cho, Toyonaka-shi, Osaka,560-0043, Japan
[39]West Virginia University, Morgantown, WV 26506, USA
[40]Center for Gravitational Waves and Cosmology, West Virginia University, Morgantown, WV 26505, USA
[41]Università di Perugia, I-06123 Perugia, Italy
[42]INFN, Sezione di Perugia, I-06123 Perugia, Italy
[43]European Gravitational Observatory (EGO), I-56021 Cascina, Pisa, Italy
[44]Syracuse University, Syracuse, NY 13244, USA
[45]SUPA, University of Glasgow, Glasgow G12 8QQ, United Kingdom
[46]LIGO Hanford Observatory, Richland, WA 99352, USA
[47]Wigner RCP, RMKI, H-1121 Budapest, Konkoly Thege Miklós út 29-33, Hungary
[48]Columbia University, New York, NY 10027, USA
[49]Stanford University, Stanford, CA 94305, USA
[50]Università di Padova, Dipartimento di Fisica e Astronomia, I-35131 Padova, Italy
[51]INFN, Sezione di Padova, I-35131 Padova, Italy
[52]MTA Eötvös University, "Lendulet" Astrophysics Research Group, Budapest 1117, Hungary
[53]Nicolaus Copernicus Astronomical Center, Polish Academy of Sciences, 00-716, Warsaw, Poland
[54]Center for Relativistic Astrophysics and School of Physics, Georgia Institute of Technology, Atlanta, GA 30332, USA
[55]University of Birmingham, Birmingham B15 2TT, United Kingdom
[56]Università degli Studi di Genova, I-16146 Genova, Italy

[57]INFN, Sezione di Genova, I-16146 Genova, Italy
[58]RRCAT, Indore MP 452013, India
[59]Faculty of Physics, Lomonosov Moscow State University, Moscow 119991, Russia
[60]SUPA, University of the West of Scotland, Paisley PA1 2BE, United Kingdom
[61]Caltech CaRT, Pasadena, CA 91125, USA
[62]University of Western Australia, Crawley, Western Australia 6009, Australia
[63]Department of Astrophysics/IMAPP, Radboud University Nijmegen, P.O. Box 9010, 6500 GL Nijmegen, The Netherlands
[64]Artemis, Université Côte d'Azur, CNRS, Observatoire Côte d'Azur, CS 34229, F-06304 Nice Cedex 4, France
[65]Institut de Physique de Rennes, CNRS, Université de Rennes 1, F-35042 Rennes, France
[66]Washington State University, Pullman, WA 99164, USA
[67]Università degli Studi di Urbino 'Carlo Bo', I-61029 Urbino, Italy
[68]INFN, Sezione di Firenze, I-50019 Sesto Fiorentino, Firenze, Italy
[69]University of Oregon, Eugene, OR 97403, USA
[70]Laboratoire Kastler Brossel, UPMC-Sorbonne Universités, CNRS, ENS-PSL Research University, Collège de France, F-75005 Paris, France
[71]Carleton College, Northfield, MN 55057, USA
[72]Astronomical Observatory Warsaw University, 00-478 Warsaw, Poland
[73]VU University Amsterdam, 1081 HV Amsterdam, The Netherlands
[74]University of Maryland, College Park, MD 20742, USA
[75]Laboratoire des Matériaux Avancés (LMA), CNRS/IN2P3, F-69622 Villeurbanne, France
[76]Université Claude Bernard Lyon 1, F-69622 Villeurbanne, France
[77]Università di Napoli 'Federico II', Complesso Universitario di Monte S.Angelo, I-80126 Napoli, Italy
[78]NASA/Goddard Space Flight Center, Greenbelt, MD 20771, USA
[79]University of Adelaide, Adelaide, South Australia 5005, Australia
[80]Tsinghua University, Beijing 100084, China
[81]Texas Tech University, Lubbock, TX 79409, USA
[82]The University of Mississippi, University, MS 38677, USA
[83]The Pennsylvania State University, University Park, PA 16802, USA
[84]National Tsing Hua University, Hsinchu City, 30013 Taiwan, Republic of China
[85]Charles Sturt University, Wagga Wagga, New South Wales 2678, Australia
[86]University of Chicago, Chicago, IL 60637, USA
[87]Kenyon College, Gambier, OH 43022, USA
[88]Korea Institute of Science and Technology Information, Daejeon 34141, Korea
[89]University of Cambridge, Cambridge CB2 1TN, United Kingdom
[90]Università di Roma 'La Sapienza', I-00185 Roma, Italy
[91]Université Libre de Bruxelles, Brussels 1050, Belgium
[92]Sonoma State University, Rohnert Park, CA 94928, USA
[93]Montana State University, Bozeman, MT 59717, USA
[94]Center for Interdisciplinary Exploration & Research in Astrophysics (CIERA), Northwestern University, Evanston, IL 60208, USA
[95]Universitat de les Illes Balears, IAC3—IEEC, E-07122 Palma de Mallorca, Spain
[96]The University of Texas Rio Grande Valley, Brownsville, TX 78520, USA
[97]Bellevue College, Bellevue, WA 98007, USA
[98]Institute for Plasma Research, Bhat, Gandhinagar 382428, India
[99]The University of Sheffield, Sheffield S10 2TN, United Kingdom
[100]California State University, Los Angeles, 5154 State University Dr, Los Angeles, CA 90032, USA
[101]Università di Trento, Dipartimento di Fisica, I-38123 Povo, Trento, Italy
[102]INFN, Trento Institute for Fundamental Physics and Applications, I-38123 Povo, Trento, Italy
[103]University of Toyama, 3190 Gofuku, Toyama-shi, Toyama, 930-8555, Japan
[104]Cardiff University, Cardiff CF24 3AA, United Kingdom
[105]Montclair State University, Montclair, NJ 07043, USA
[106]Canadian Institute for Theoretical Astrophysics, University of Toronto, Toronto, Ontario M5S 3H8, Canada
[107]School of Mathematics, University of Edinburgh, Edinburgh EH9 3FD, United Kingdom
[108]University and Institute of Advanced Research, Gandhinagar, Gujarat 382007, India
[109]IISER-TVM, CET Campus, Trivandrum Kerala 695016, India

[110]University of Szeged, Dóm tér 9, Szeged 6720, Hungary
[111]Embry-Riddle Aeronautical University, Prescott, AZ 86301, USA
[112]Tata Institute of Fundamental Research, Mumbai 400005, India
[113]INAF, Osservatorio Astronomico di Capodimonte, I-80131, Napoli, Italy
[114]University of Michigan, Ann Arbor, MI 48109, USA
[115]High Energy Accelerator Research Organization , 1-1, Oho,Tsukuba-shi, Ibaraki, 305-0801, Japan
[116]Rochester Institute of Technology, Rochester, NY 14623, USA
[117]NCSA, University of Illinois at Urbana-Champaign, Urbana, IL 61801, USA
[118]Center for Gravitational Physics, Yukawa Institute for Theoretical Physics, Kyoto University, Kyoto 606-8502, Japan
[119]University of Białystok, 15-424 Białystok, Poland
[120]SUPA, University of Strathclyde, Glasgow G1 1XQ, United Kingdom
[121]University of Southampton, Southampton SO17 1BJ, United Kingdom
[122]Osaka City University, Department of Physics, 3-3-138, Sugimoto-cho, Sumiyosi-ku, Osaka-shi, Osaka, 558-8585, Japan
[123]University of Washington Bothell, 18115 Campus Way NE, Bothell, WA 98011, USA
[124]Institute of Applied Physics, Nizhny Novgorod, 603950, Russia
[125]Korea Astronomy and Space Science Institute (KASI), 776, Daedeokdae-ro, Yuseong-gu, Daejeon, 34055, Republic of Korea
[126]National Institute for Mathematical Sciences, Daejeon 34047, Korea
[127]Inje University, 197 Inje-ro, Gimhae-si, 50834 Korea
[128]Myongji University, Yongin 449-728, Korea
[129]Pusan National University, Busan 609-735, Korea
[130]Seoul National University, Seoul 151-742, Korea
[131]Hiroshima University, Department of Physical Science, 1-3-1, Kagamiyama, Higashihiroshima-shi, Hiroshima, 739-8526, Japan
[132]Fukuoka University, Department of Applied Physics, Fukuoka, Jonan, Nanakuma, 814-0180, Japan
[133]NCBJ, 05-400 Świerk-Otwock, Poland
[134]Institute of Mathematics, Polish Academy of Sciences, 00656 Warsaw, Poland
[135]The School of Physics & Astronomy, Monash University, Clayton 3800, Victoria, Australia
[136]Hanyang University, Seoul 133-791, Korea
[137]The Chinese University of Hong Kong, Shatin, NT, Hong Kong
[138]University of Alabama in Huntsville, Huntsville, AL 35899, USA
[139]ESPCI, CNRS, F-75005 Paris, France
[140]University of Minnesota, Minneapolis, MN 55455, USA
[141]The Institute of Statistical Mathematics, Department of Mathematical Analysis and Statistical Inference, 10-3 Midori-cho, Tachikawa, Tokyo 190-8562, Japan
[142]Università di Camerino, Dipartimento di Fisica, I-62032 Camerino, Italy
[143]Tohoku University, Sendai, Miyagi 982-0826, Japan
[144]Southern University and A&M College, Baton Rouge, LA 70813, USA
[145]The University of Melbourne, Parkville, Victoria 3010, Australia
[146]College of William and Mary, Williamsburg, VA 23187, USA
[147]Instituto de Física Teórica, University Estadual Paulista/ICTP South American Institute for Fundamental Research, São Paulo SP 01140-070, Brazil
[148]The Kyoto University, Disaster Prevention Research Institute, Gokasho, Uji, Kyoto, 611-0011, Japan
[149]National Institute of Information and Communications Technology, The Applied Electromagnetic Research Institute , 4-2-1, Nukuikita-machi, Koganei-shi, Tokyo, 184-8795, Japan
[150]Kyoto University, Department of Physics, Astronomy, Oiwake-cho, KitaShirakawa, Sakyou-ku, Kyoto-shi, Kyoto, 606-8502, Japan
[151]National Tsing Hua University, Department of Physics, No. 101, Section 2, Kuang-Fu Road, Hsinchu, Taiwan 30013, ROC
[152]University of Shanghai for Science and Technology, School of Optical-Electrical and Computer Engineering, 516, Jun Gong Rd., Shanghai 200093, P. R. China
[153]Whitman College, 345 Boyer Avenue, Walla Walla, WA 99362 USA
[154]Niigata University, Faculty of Engineering, 8050, Ikarashi-2-no-cho, Nishi-ku, Niigata-shi, Niigata, 950-2181, Japan
[155]Sokendai (The Graduate University for Advanced Studies), 2-21-1, Ohsawa, Mitaka-shi, Tokyo, 181-8588, Japan

[156]Niigata University, Graduate School of Science and Technology, 8050, Ikarashi-2-no-cho, Nishi-ku, Niigata-shi, Niigata, 950-2181, Japan
[157]Université de Lyon, F-69361 Lyon, France
[158]Hobart and William Smith Colleges, Geneva, NY 14456, USA
[159]Janusz Gil Institute of Astronomy, University of Zielona Góra, 65-265 Zielona Góra, Poland
[160]Kyushu University, Faculty of Arts and Science, 744, Motooka, Nishi-ku, Fukuoka, 819-0395, Japan
[161]Waseda University, Department of Physics, 3-4-1, Okubo, Shinjuku, Tokyo, 169-8555, Japan
[162]Nagaoka University of Technology, Department of Information Science and Control Engineering, 1603-1 Kamitomioka, Nagaoka, Niigata 940-2188 Japan
[163]King's College London, University of London, London WC2R 2LS, United Kingdom
[164]IISER-Kolkata, Mohanpur, West Bengal 741252, India
[165]Nagaoka University of Technology, Department of Information & Management Systems Engineering, 1603-1 Kamitomioka, Nagaoka, Niigata 940-2188 Japan
[166]Hosei University, The Graduate School of Science and Engineering, Kajino-cho 3-7-2, Koganei-shi, Tokyo 184-8584, Japan
[167]Toho University, Faculty of Science, 2-2-1 Miyama, Funabashi-shi, Chiba, Japan
[168]Indian Institute of Technology, Gandhinagar Ahmedabad Gujarat 382424, India
[169]Institute for Molecular Science, National Institutes of Natural Sciences, 38 Nishigo-Naka, Myodaiji, Okazaki 444-8585, Japan
[170]Institute for Quantum Studies, Chapman University, 1 University Dr., Orange, CA 92866 USA
[171]Andrews University, Berrien Springs, MI 49104, USA
[172]National Institutes of Natural Sciences, The Device Engineering and Applied Physics Research Division, 322-6 Oroshi-cho, Toki city, GIFU Prefecture, 509-5292, Japan
[173]National Institute of Advanced Industrial Science and Technology, Metrology Institute of Japan , 1-1-1, Umezono, Tsukuba-shi, Ibaraki, 305-8568, Japan
[174]Università di Siena, I-53100 Siena, Italy
[175]National Defense Academy of Japan, Department of Communications Engineering, Hashirimizu 1-10-20, Yokosuka-shi, Kanagawa-Pref, 239-8686, Japan
[176]Trinity University, San Antonio, TX 78212, USA
[177]Physics and Astronomy, Sejong University, 209 Neungdong-ro, Gwangjin-gu, 143-747 Seoul, South Korea
[178]University of Washington, Seattle, WA 98195, USA
[179]Abilene Christian University, Abilene, TX 79699, USA
[180]Department of Physics, Korea University, 145, Anam-ro, Seongbuk-gu, Seoul 02841, Korea

References

1. G.M. Harry, Class. Quantum Grav. **27**, 084006 (2010). DOI 10.1088/0264-9381/27/8/084006
2. J. Aasi, et al., Class. Quantum Grav. **32**, 074001 (2015). DOI 10.1088/0264-9381/32/7/074001. arXiv:1411.4547
3. F. Acernese, et al., Advanced Virgo baseline design. Tech. Rep. VIR-027A-09, Cascina (2009). URL `https://tds.ego-gw.it/ql/?c=6589`
4. T. Accadia, et al., Advanced Virgo technical design report. Tech. Rep. VIR-0128A-12, Cascina (2012). URL `https://tds.ego-gw.it/ql/?c=8940`
5. F. Acernese, et al., Class. Quantum Grav. **32**(2), 024001 (2015). DOI 10.1088/0264-9381/32/2/024001. arXiv:1408.3978
6. K. Somiya, Class. Quantum Grav. **29**, 124007 (2012). DOI 10.1088/0264-9381/29/12/124007. arXiv:1111.7185
7. Y. Aso, et al., Phys. Rev. D **88**(4), 043007 (2013). DOI 10.1103/PhysRevD.88.043007. arXiv:1306.6747
8. B.P. Abbott, et al., Phys. Rev. Lett. **116**(6), 061102 (2016). DOI 10.1103/PhysRevLett.116.061102. arXiv:1602.03837
9. B.P. Abbott, et al., Astrophys. J. Lett. **826**(1), L13 (2016). DOI 10.3847/2041-8205/826/1/L13
10. S. Adrian-Martinez, et al., Phys. Rev. D **93**(12), 122010 (2016). DOI 10.1103/PhysRevD.93.122010. arXiv:1602.05411
11. A. Albert, et al., Phys. Rev. D **96**(2), 022005 (2017). DOI 10.1103/PhysRevD.96.022005. arXiv:1703.06298
12. B.P. Abbott, et al., The LSC–Virgo white paper on gravitational wave searches and astrophysics (2016–2017 edition). Tech. Rep. LIGO-T1600115-v6, Pasadena, CA (2016). URL `https://dcc.ligo.org/LIGO-T1600115/public`
13. B.D. Metzger, E. Berger, Astrophys. J. **746**, 48 (2012). DOI 10.1088/0004-637X/746/1/48. arXiv:1108.6056
14. B. Patricelli, et al., J. Cosmol. Astropart. Phys. **1611**(11), 056 (2016). DOI 10.1088/1475-7516/2016/11/056. arXiv:1606.06124
15. V. Paschalidis, Class. Quantum Grav. **34**(8), 084002 (2017). DOI 10.1088/1361-6382/aa61ce. arXiv:1611.01519
16. S. Rosswog, et al., Class. Quantum Grav. **34**(10), 104001 (2017). DOI 10.1088/1361-6382/aa68a9. arXiv:1611.09822
17. B.P. Abbott, et al., Phys. Rev. Lett. **116**(24), 241103 (2016). DOI 10.1103/PhysRevLett.116.241103. arXiv:1606.04855
18. B.P. Abbott, et al., Phys. Rev. X **6**(4), 041015 (2016). DOI 10.1103/PhysRevX.6.041015. arXiv:1606.04856
19. B. Abbott, et al., Phys. Rev. Lett. **118**(22), 221101 (2017). DOI 10.1103/PhysRevLett.118.221101. arXiv:1706.01812
20. J. Centrella, et al., Rev. Mod. Phys. **82**, 3069 (2010). DOI 10.1103/RevModPhys.82.3069. arXiv:1010.5260
21. J.D. Schnittman, Class. Quantum Grav. **30**, 244007 (2013). DOI 10.1088/0264-9381/30/24/244007. arXiv:1307.3542
22. R. Perna, D. Lazzati, B. Giacomazzo, Astrophys. J. Lett. **821**(1), L18 (2016). DOI 10.3847/2041-8205/821/1/L18. arXiv:1602.05140
23. A. Janiuk, M. Bejger, S. Charzyński, P. Sukova, New Astron. **51**, 7 (2017). DOI 10.1016/j.newast.2016.08.002. arXiv:1604.07132
24. I. Bartos, B. Kocsis, Z. Haiman, S. Márka, Astrophys. J. **835**(2), 165 (2017). DOI 10.3847/1538-4357/835/2/165. arXiv:1602.03831
25. S.E. Woosley, Astrophys. J. Lett. **824**(1), L10 (2016). DOI 10.3847/2041-8205/824/1/L10. arXiv:1603.00511
26. N.C. Stone, B.D. Metzger, Z. Haiman, Mon. Not. R. Astron. Soc. **464**(1), 946 (2017). DOI 10.1093/mnras/stw2260. arXiv:1602.04226
27. L. Blanchet, Living Rev. Relat. **17**, 2 (2014). DOI 10.12942/lrr-2014-2. arXiv:1310.1528
28. M. Pitkin, S. Reid, S. Rowan, J. Hough, Living Rev. Relat. **14**, 5 (2011). DOI 10.12942/lrr-2011-5. arXiv:1102.3355
29. B. Sathyaprakash, B.F. Schutz, Living Rev. Relat. **12**, 2 (2009). DOI 10.12942/lrr-2009-2. arXiv:0903.0338

30. J. Aasi, et al., Living Rev. Relat. **19**, 1 (2016). DOI 10.1007/lrr-2016-1. arXiv:1304.0670v3
31. J. Abadie, et al., LSC and Virgo policy on releasing gravitational wave triggers to the public in the advanced detectors era. Tech. Rep. LIGO M1200055-v2 / VIR-0173A-12, Pasadena, CA (2012). URL `https://dcc.ligo.org/LIGO-M1200055-v2/public`
32. J. Aasi, et al., Open call for partnership for the EM identification and follow-up of GW candidate events. Tech. Rep. LIGO M1300550-v3 / VIR-0494E-13, Pasadena, CA (2013). URL `https://dcc.ligo.org/LIGO-M1300550-v8/public`
33. L. Finn, D. Chernoff, Phys. Rev. D **47**, 2198 (1993). DOI 10.1103/PhysRevD.47.2198. arXiv:gr-qc/9301003
34. D.E. Holz, H.S. Chen, Cosmological versions of horizon distance, sensitive volume, and all that. Tech. Rep. LIGO-P1600071, Pasadena, CA (2017). URL `https://dcc.ligo.org/LIGO-P1600071/public`
35. B. Iyer, et al., LIGO-India. Tech. Rep. M1100296-v2, India (2011). URL `https://dcc.ligo.org/LIGO-M1100296/public`
36. B.P. Abbott, et al., Phys. Rev. Lett. **116**(13), 131103 (2016). DOI 10.1103/PhysRevLett.116.131103. arXiv:1602.03838
37. H. Lück, et al., **228**, 012012 (2010). DOI 10.1088/1742-6596/228/1/012012. arXiv:1004.0339
38. K.L. Dooley, et al., Class. Quantum Grav. **33**, 075009 (2016). DOI 10.1088/0264-9381/33/7/075009. arXiv:1510.00317
39. C. Affeldt, et al., Class. Quantum Grav. **31**(22), 224002 (2014). DOI 10.1088/0264-9381/31/22/224002
40. H. Lück, et al., J. Phys. Conf. Ser. **228**, 012012 (2010). DOI 10.1088/1742-6596/228/1/012012. arXiv:1004.0339
41. H. Wittel, et al., Class. Quantum Grav. **31**, 065008 (2014). DOI 10.1088/0264-9381/31/6/065008. arXiv:1311.5367
42. K.L. Dooley, J. Phys. Conf. Ser. **610**(1), 012015 (2015). DOI 10.1088/1742-6596/610/1/012015. arXiv:1411.6588
43. J. Abadie, et al., Nature Phys. **7**, 962 (2011). DOI 10.1038/nphys2083. arXiv:1109.2295
44. H. Grote, et al., Phys. Rev. Lett. **110**(18), 181101 (2013). DOI 10.1103/PhysRevLett.110.181101. arXiv:1302.2188
45. J. Aasi, et al., Nature Photon. **7**, 613 (2013). DOI 10.1038/nphoton.2013.177. arXiv:1310.0383
46. S. Hild, et al., LIGO 3 Strawman Design, Team Red. Tech. Rep. LIGO-T1200046-v1, Pasadena, CA (2012). URL `https://dcc.ligo.org/LIGO-T1200046/public`
47. J. Miller, et al., Phys. Rev. D **91**, 062005 (2015). DOI 10.1103/PhysRevD.91.062005. arXiv:1410.5882
48. J. Aasi, et al., Instrument science white paper. Tech. Rep. LIGO-T1400316-v4, Pasadena, CA (2015). URL `https://dcc.ligo.org/LIGO-T1400316/public`
49. M. Punturo, et al., Class. Quantum Grav. **27**, 194002 (2010). DOI 10.1088/0264-9381/27/19/194002
50. S. Hild, et al., Class. Quantum Grav. **28**, 094013 (2011). DOI 10.1088/0264-9381/28/9/094013. arXiv:1012.0908
51. B. Sathyaprakash, et al., Class. Quantum Grav. **29**, 124013 (2012). DOI 10.1088/0264-9381/29/12/124013. arXiv:1206.0331
52. B.P. Abbott, et al., Class. Quantum Grav. **34**(4), 044001 (2017). DOI 10.1088/1361-6382/aa51f4. arXiv:1607.08697
53. P. Amaro-Seoane, et al., Class. Quantum Grav. **29**, 124016 (2012). DOI 10.1088/0264-9381/29/12/124016. arXiv:1202.0839
54. P. Amaro-Seoane, et al., GW Notes **6**, 4 (2013). arXiv:1201.3621
55. A. Sesana, Phys. Rev. Lett. **116**(23), 231102 (2016). DOI 10.1103/PhysRevLett.116.231102. arXiv:1602.06951
56. S. Vitale, Phys. Rev. Lett. **117**(5), 051102 (2016). DOI 10.1103/PhysRevLett.117.051102. arXiv:1605.01037
57. A. Nishizawa, E. Berti, A. Klein, A. Sesana, Phys. Rev. D **94**(6), 064020 (2016). DOI 10.1103/PhysRevD.94.064020. arXiv:1605.01341
58. A. Nishizawa, A. Sesana, E. Berti, A. Klein, Mon. Not. R. Astron. Soc. **465**(4), 4375 (2016). DOI 10.1093/mnras/stw2993. arXiv:1606.09295
59. K. Breivik, et al., Astrophys. J. Lett. **830**(1), L18 (2016). DOI 10.3847/2041-8205/830/1/L18. arXiv:1606.09558
60. E. Barausse, N. Yunes, K. Chamberlain, Phys. Rev. Lett. **116**(24), 241104 (2016). DOI 10.1103/PhysRevLett.116.241104. arXiv:1603.04075

61. S. Klimenko, et al., Phys. Rev. D **83**, 102001 (2011). DOI 10.1103/PhysRevD.83.102001. arXiv: 1101.5408
62. J. Veitch, et al., Phys. Rev. D **85**, 104045 (2012). DOI 10.1103/PhysRevD.85.104045. arXiv: 1201.1195
63. S. Nissanke, M. Kasliwal, A. Georgieva, Astrophys. J. **767**, 124 (2013). DOI 10.1088/0004-637X/ 767/2/124. arXiv:1210.6362
64. C.L. Rodriguez, et al., Astrophys. J. **784**, 119 (2014). DOI 10.1088/0004-637X/784/2/119. arXiv: 1309.3273
65. B.P. Abbott, et al., Phys. Rev. D **93**(12), 122003 (2016). DOI 10.1103/PhysRevD.93.122003. arXiv: 1602.03839
66. B.P. Abbott, et al., Phys. Rev. D **93**(12), 122004 (2016). DOI 10.1103/PhysRevD.93.122004. arXiv: 1602.03843
67. B.P. Abbott, et al., Phys. Rev. D **95**(4), 042003 (2017). DOI 10.1103/PhysRevD.95.042003. arXiv: 1611.02972
68. B.P. Abbott, et al., Astrophys. J. Lett. **832**(2), L21 (2016). DOI 10.3847/2041-8205/832/2/L21. arXiv:1607.07456
69. B.P. Abbott, et al., Astrophys. J. **841**(2), 89 (2017). DOI 10.3847/1538-4357/aa6c47. arXiv:1611. 07947
70. B.P. Abbott, et al., Phys. Rev. Lett. **116**(24), 241102 (2016). DOI 10.1103/PhysRevLett.116.241102. arXiv:1602.03840
71. B.P. Abbott, et al., Phys. Rev. D **96**(2), 022001 (2017). DOI 10.1103/PhysRevD.96.022001. arXiv: 1704.04628
72. J.A. Faber, F.A. Rasio, Living Rev. Rel. **15**, 8 (2012). DOI 10.12942/lrr-2012-8. arXiv:1204.3858
73. J. Abadie, et al., Class. Quantum Grav. **27**, 173001 (2010). DOI 10.1088/0264-9381/27/17/173001. arXiv:1003.2480
74. C. Kim, B.B.P. Perera, M.A. McLaughlin, Mon. Not. Roy. Astron. Soc. **448**(1), 928 (2013). DOI 10.1093/mnras/stu2729. arXiv:1308.4676
75. M. Dominik, et al., Astrophys. J. **806**(2), 263 (2015). DOI 10.1088/0004-637X/806/2/263. arXiv: 1405.7016
76. E. Vangioni, S. Goriely, F. Daigne, P. Franois, K. Belczynski, Mon. Not. Roy. Astron. Soc. **455**(1), 17 (2016). DOI 10.1093/mnras/stv2296. arXiv:1501.01115
77. S.E. de Mink, K. Belczynski, Astrophys. J. **814**(1), 58 (2015). DOI 10.1088/0004-637X/814/1/58. arXiv:1506.03573
78. Z.P. Jin, et al., Astrophys. J. Lett. **811**(2), L22 (2015). DOI 10.1088/2041-8205/811/2/L22. arXiv: 1507.07206
79. W.f. Fong, E. Berger, R. Margutti, B.A. Zauderer, Astrophys. J. **815**(2), 102 (2015). DOI 10.1088/ 0004-637X/815/2/102. arXiv:1509.02922
80. C.L. Rodriguez, et al., Phys. Rev. Lett. **115**(5), 051101 (2015). DOI 10.1103/PhysRevLett.115.051101. arXiv:1505.00792
81. B.P. Abbott, et al., Astrophys. J. Lett. **818**(2), L22 (2016). DOI 10.3847/2041-8205/818/2/L22. arXiv:1602.03846
82. X. Li, Y.M. Hu, Z.P. Jin, Y.Z. Fan, D.M. Wei, Astrophys. J. Lett. **844**(2), L22 (2017). DOI 10.3847/ 2041-8213/aa7fb2. arXiv:1611.01760
83. L. Lindblom, B.J. Owen, D.A. Brown, Phys. Rev. D **78**, 124020 (2008). DOI 10.1103/PhysRevD.78. 124020. arXiv:0809.3844
84. A. Buonanno, B. Iyer, E. Ochsner, Y. Pan, B.S. Sathyaprakash, Phys. Rev. D **80**, 084043 (2009). DOI 10.1103/PhysRevD.80.084043. arXiv:0907.0700
85. D.A. Brown, I. Harry, A. Lundgren, A.H. Nitz, Phys. Rev. D **86**, 084017 (2012). DOI 10.1103/ PhysRevD.86.084017. arXiv:1207.6406
86. J.S. Read, et al., Phys. Rev. D **88**, 044042 (2013). DOI 10.1103/PhysRevD.88.044042. arXiv: 1306.4065
87. I. Harry, S. Privitera, A. Bohé, A. Buonanno, Phys. Rev. D **D94**(2), 024012 (2016). DOI 10.1103/ PhysRevD.94.024012. arXiv:1603.02444
88. A.H. Nitz, et al., Phys. Rev. D **88**(12), 124039 (2013). DOI 10.1103/PhysRevD.88.124039. arXiv: 1307.1757
89. I.W. Harry, et al., Phys. Rev. D **89**(2), 024010 (2014). DOI 10.1103/PhysRevD.89.024010. arXiv: 1307.3562
90. T. Dal Canton, A.P. Lundgren, A.B. Nielsen, Phys. Rev. D **91**(6), 062010 (2015). DOI 10.1103/ PhysRevD.91.062010. arXiv:1411.6815

91. A. Taracchini, et al., Phys. Rev. D **89**(6), 061502 (2014). DOI 10.1103/PhysRevD.89.061502. arXiv: 1311.2544
92. Y. Pan, et al., Phys. Rev. D **89**(8), 084006 (2014). DOI 10.1103/PhysRevD.89.084006. arXiv: 1307.6232
93. P. Schmidt, F. Ohme, M. Hannam, Phys. Rev. D **91**(2), 024043 (2015). DOI 10.1103/PhysRevD.91. 024043. arXiv:1408.1810
94. S. Khan, et al., Phys. Rev. D **93**(4), 044007 (2016). DOI 10.1103/PhysRevD.93.044007. arXiv: 1508.07253
95. J.C. Bustillo, P. Laguna, D. Shoemaker, Phys. Rev. D **95**(10), 104038 (2017). DOI 10.1103/PhysRevD. 95.104038. arXiv:1612.02340
96. S. Klimenko, I. Yakushin, A. Mercer, G. Mitselmakher, Class. Quantum Grav. **25**, 114029 (2008). DOI 10.1088/0264-9381/25/11/114029. arXiv:0802.3232
97. P.J. Sutton, et al., New J. Phys. **12**, 053034 (2010). DOI 10.1088/1367-2630/12/5/053034. arXiv: 0908.3665
98. E. Chassande-Mottin, M. Miele, S. Mohapatra, L. Cadonati, Class. Quantum Grav. **27**, 194017 (2010). DOI 10.1088/0264-9381/27/19/194017. arXiv:1005.2876
99. E. Thrane, et al., Phys. Rev. D **83**, 083004 (2011). DOI 10.1103/PhysRevD.83.083004. arXiv: 1012.2150
100. T.S. Adams, et al., Phys. Rev. D **88**, 062006 (2013). DOI 10.1103/PhysRevD.88.062006. arXiv: 1305.5714
101. E. Thrane, M. Coughlin, Phys. Rev. D **88**(8), 083010 (2013). DOI 10.1103/PhysRevD.88.083010. arXiv:1308.5292
102. N.J. Cornish, T.B. Littenberg, Class. Quantum Grav. **32**(13), 135012 (2015). DOI 10.1088/0264-9381/ 32/13/135012. arXiv:1410.3835
103. E. Thrane, V. Mandic, N. Christensen, Phys. Rev. S **91**(10), 104021 (2015). DOI 10.1103/PhysRevD. 91.104021. arXiv:1501.06648
104. J.B. Kanner, et al., Phys. Rev. D **93**(2), 022002 (2016). DOI 10.1103/PhysRevD.93.022002. arXiv: 1509.06423
105. J. Abadie, et al., Astron. Astrophys. **539**, A124 (2012). DOI 10.1051/0004-6361/201118219. arXiv: 1109.3498
106. J. Abadie, et al., Astron. Astrophys. **541**, A155 (2012). DOI 10.1051/0004-6361/201218860. arXiv: 1112.6005
107. P. Evans, et al., Astrophys. J. Suppl. **203**, 28 (2012). DOI 10.1088/0067-0049/203/2/28. arXiv: 1205.1124
108. B.P. Abbott, et al., Astrophys. J. Suppl. **225**(1), 8 (2016). DOI 10.3847/0067-0049/225/1/8. arXiv: 1604.07864
109. M. Soares-Santos, et al., Astrophys. J. Lett. **823**(2), L33 (2016). DOI 10.3847/2041-8205/823/2/L33. arXiv:1602.04198
110. J. Annis, et al., Astrophys. J. Lett. **823**(2), L34 (2016). DOI 10.3847/2041-8205/823/2/L34. arXiv: 1602.04199
111. V. Connaughton, et al., Astrophys. J. Lett. **826**(1), L6 (2016). DOI 10.3847/2041-8205/826/1/L6. arXiv:1602.03920
112. M. Ackermann, et al., Astrophys. J. Lett. **823**(1), L2 (2016). DOI 10.3847/2041-8205/823/1/L2. arXiv:1602.04488
113. V. Savchenko, et al., Astrophys. J. Lett. **820**(2), L36 (2016). DOI 10.3847/2041-8205/820/2/L36. arXiv:1602.04180
114. M.M. Kasliwal, et al., Astrophys. J. Lett. **824**(2), L24 (2016). DOI 10.3847/2041-8205/824/2/L24. arXiv:1602.08764
115. N.T. Palliyaguru, et al., Astrophys. J. Lett. **829**(2), L28 (2016). DOI 10.3847/2041-8205/829/2/L28. arXiv:1608.06518
116. K. Hurley, et al., Astrophys. J. Lett. **829**(1), L12 (2016). DOI 10.3847/2041-8205/829/1/L12
117. T. Morokuma, et al., Publ. Astron. Soc. Jpn **68**(4), L9 (2016). DOI 10.1093/pasj/psw061. arXiv: 1605.03216
118. C.M. Copperwheat, et al., Mon. Not. Roy. Astron. Soc. **462**(4), 3528 (2016). DOI 10.1093/mnras/ stw1849. arXiv:1606.04574
119. V.M. Lipunov, et al., Mon. Not. Roy. Astron. Soc. **465**(3), 3656 (2017). DOI 10.1093/mnras/stw2669. arXiv:1605.01607
120. N. Kawai, et al. X-ray upper limits of GW150914 with MAXI (2017). arXiv:1708.01342

121. S.J. Smartt, et al., Mon. Not. Roy. Astron. Soc. **462**, 4094 (2016). DOI 10.1093/mnras/stw1893. arXiv:1602.04156
122. P.A. Evans, et al., Mon. Not. Roy. Astron. Soc. Lett. **460**, L40 (2016). DOI 10.1093/mnrasl/slw065. arXiv:1602.03868
123. M.C. Diaz, et al., Astrophys. J. Lett. **828**(2), L16 (2016). DOI 10.3847/2041-8205/828/2/L16. arXiv:1607.07850
124. E. Troja, A.M. Read, A. Tiengo, R. Salvaterra, Astrophys. J. Lett. **822**(1), L8 (2016). DOI 10.3847/2041-8205/822/1/L8. arXiv:1603.06585
125. M. Tavani, et al., Astrophys. J. Lett. **825**(1), L4 (2016). DOI 10.3847/2041-8205/825/1/L4. arXiv:1604.00955
126. Z. Bagoly, et al., Astron. Astrophys. **593**, L10 (2016). DOI 10.1051/0004-6361/201628569. arXiv:1603.06611
127. A. Loeb, Astrophys. J. Lett. **819**(2), L21 (2016). DOI 10.3847/2041-8205/819/2/L21. arXiv:1602.04735
128. X. Li, et al., Astrophys. J. Lett. **827**(1), L16 (2016). DOI 10.3847/2041-8205/827/1/L16. arXiv:1602.04460
129. R. Yamazaki, K. Asano, Y. Ohira, Progr. Theor. Exp. Phys. **2016**(5), 051E01 (2016). DOI 10.1093/ptep/ptw042. arXiv:1602.05050
130. G. Ryan, A. MacFadyen, Astrophys. J. **835**(2), 199 (2017). DOI 10.3847/1538-4357/835/2/199. arXiv:1611.00341
131. K. Murase, K. Kashiyama, P. Mészáros, I. Shoemaker, N. Senno, Astrophys. J. Lett. **822**(1), L9 (2016). DOI 10.3847/2041-8205/822/1/L9. arXiv:1602.06938
132. B.J. Morsony, J.C. Workman, D.M. Ryan, Astrophys. J. Lett. **825**(2), L24 (2016). DOI 10.3847/2041-8205/825/2/L24. arXiv:1602.05529
133. L. Dai, J.C. McKinney, M.C. Miller, Mon. Not. R. Astron. Soc. Lett. **470**(1), L92 (2017). DOI 10.1093/mnrasl/slx086. arXiv:1611.00764
134. M. Lyutikov. Fermi GBM signal contemporaneous with GW150914 – an unlikely association (2016). arXiv:1602.07352
135. S.E. de Mink, A. King, Astrophys. J. Lett. **839**(1), L7 (2017). DOI 10.3847/2041-8213/aa67f3. arXiv:1703.07794
136. A. Gando, et al., Astrophys. J. Lett. **829**(2), L34 (2016). DOI 10.3847/2041-8205/829/2/L34. arXiv:1606.07155
137. A. Aab, et al., Phys. Rev. D **94**(12), 122007 (2016). DOI 10.1103/PhysRevD.94.122007. arXiv:1608.07378
138. K. Abe, et al., Astrophys. J. Lett. **830**(1), L11 (2016). DOI 10.3847/2041-8205/830/1/L11. arXiv:1608.08745
139. M. Agostini, et al. A search for low-energy neutrinos correlated with gravitational wave events GW150914, GW151226 and GW170104 with the Borexino detector (2017). arXiv:1706.10176
140. P.S. Cowperthwaite, et al., Astrophys. J. Lett. **826**, L29 (2016). DOI 10.3847/2041-8205/826/2/L29. arXiv:1606.04538
141. S.J. Smartt, et al., Astrophys. J. Lett. **827**(2), L40 (2016). DOI 10.3847/2041-8205/827/2/L40. arXiv:1606.04795
142. J.L. Racusin, et al., Astrophys. J. **835**(1), 82 (2017). DOI 10.3847/1538-4357/835/1/82. arXiv:1606.04901
143. P.A. Evans, et al., Mon. Not. Roy. Astron. Soc. **462**(2), 1591 (2016). DOI 10.1093/mnras/stw1746. arXiv:1606.05001
144. O. Adriani, et al., Astrophys. J. Lett. **829**(1), L20 (2016). DOI 10.3847/2041-8205/829/1/L20. arXiv:1607.00233
145. M. Yoshida, et al., Publ. Astron. Soc. Jpn **69**(1), 12 (2017). DOI 10.1093/pasj/psw113. arXiv:1611.01588
146. M. Serino, et al. X-ray upper limits of GW151226 with MAXI (2017). arXiv:1708.01352
147. V. Bhalerao, et al., Astrophys. J. **845**(2), 152 (2017). DOI 10.3847/1538-4357/aa81d2. arXiv:1706.00024
148. F. Verrecchia, et al. AGILE Observations of the Gravitational Wave Source GW170104 (2017). arXiv:1706.00029
149. A. Corsi, et al. iPTF17cw: An engine-driven supernova candidate discovered independent of a gamma-ray trigger (2017). arXiv:1706.00045
150. B. Stalder, et al. Observations of the GRB afterglow ATLAS17aeu and its possible association with GW170104 (2017). arXiv:1706.00175

151. Fermi observations of the LIGO event GW170104 (2017). arXiv:1706.00199
152. V. Savchenko, et al. INTEGRAL observations of GW170104 (2017). arXiv:1707.03719
153. B.S. Sathyaprakash, S.V. Dhurandhar, Phys. Rev. D **44**, 3819 (1991). DOI 10.1103/PhysRevD.44.3819
154. B.J. Owen, Phys. Rev. D **53**, 6749 (1996). DOI 10.1103/PhysRevD.53.6749. arXiv:gr-qc/9511032
155. B.J. Owen, B. Sathyaprakash, Phys. Rev. D **60**, 022002 (1999). DOI 10.1103/PhysRevD.60.022002. arXiv:gr-qc/9808076
156. S. Babak, R. Balasubramanian, D. Churches, T. Cokelaer, B.S. Sathyaprakash, Class. Quantum Grav. **23**, 5477 (2006). DOI 10.1088/0264-9381/23/18/002. arXiv:gr-qc/0604037
157. T. Cokelaer, Phys. Rev. D **76**, 102004 (2007). DOI 10.1103/PhysRevD.76.102004. arXiv:0706.4437
158. R. Prix, Class. Quantum Grav. **24**, S481 (2007). DOI 10.1088/0264-9381/24/19/S11. arXiv:0707.0428
159. I.W. Harry, B. Allen, B.S. Sathyaprakash, Phys. Rev. D **80**, 104014 (2009). DOI 10.1103/PhysRevD.80.104014. arXiv:0908.2090
160. P. Ajith, N. Fotopoulos, S. Privitera, A. Neunzert, A.J. Weinstein, Phys. Rev. D **89**(8), 084041 (2014). DOI 10.1103/PhysRevD.89.084041. arXiv:1210.6666
161. C. Capano, I. Harry, S. Privitera, A. Buonanno, Phys. Rev. D **93**(12), 124007 (2016). DOI 10.1103/PhysRevD.93.124007. arXiv:1602.03509
162. T. Dal Canton, I.W. Harry. Designing a template bank to observe compact binary coalescences in Advanced LIGO's second observing run (2017). arXiv:1705.01845
163. J. Abadie, et al., Phys. Rev. D **81**, 102001 (2010). DOI 10.1103/PhysRevD.85.089905. arXiv:1002.1036
164. S. Babak, et al., Phys. Rev. D **87**, 024033 (2013). DOI 10.1103/PhysRevD.87.024033. arXiv:1208.3491
165. J. Abadie, et al., Phys. Rev. D **85**, 122007 (2012). DOI 10.1103/PhysRevD.85.122007. arXiv:1202.2788
166. B.P. Abbott, et al., Phys. Rev. D **93**(4), 042005 (2016). DOI 10.1103/PhysRevD.93.042005. arXiv:1511.04398
167. C. Capano, et al. Systematic errors in estimation of gravitational-wave candidate significance (2016). arXiv:1601.00130
168. C. Messick, et al., Phys. Rev. D **95**(4), 042001 (2017). DOI 10.1103/PhysRevD.95.042001. arXiv:1604.04324
169. A.H. Nitz, T. Dent, T. Dal Canton, S. Fairhurst, D.A. Brown. Detecting binary compact-object mergers with gravitational waves: Understanding and Improving the sensitivity of the PyCBC search (2017). arXiv:1705.01513
170. B.P. Abbott, et al., Astrophys. J. Lett. **833**, 1 (2016). DOI 10.3847/2041-8205/833/1/L1. arXiv:1602.03842
171. B.P. Abbott, et al., Astrophys. J. Suppl. **227**(2), 14 (2016). DOI 10.3847/0067-0049/227/2/14. arXiv:1606.03939
172. J. Aasi, et al., Class. Quantum Grav. **29**, 155002 (2012). DOI 10.1088/0264-9381/29/15/155002. arXiv:1203.5613
173. J. Aasi, et al., Class. Quantum Grav. **32**(11), 115012 (2015). DOI 10.1088/0264-9381/32/11/115012. arXiv:1410.7764
174. B.P. Abbott, et al., Class. Quantum Grav. **33**(13), 134001 (2016). DOI 10.1088/0264-9381/33/13/134001. arXiv:1602.03844
175. A. Effler, et al., Class. Quantum Grav. **32**(3), 035017 (2015). DOI 10.1088/0264-9381/32/3/035017. arXiv:1409.5160
176. B. Allen, Phys. Rev. D **71**, 062001 (2005). DOI 10.1103/PhysRevD.71.062001. arXiv:gr-qc/0405045
177. K. Cannon, C. Hanna, J. Peoples. Likelihood-Ratio Ranking Statistic for Compact Binary Coalescence Candidates with Rate Estimation (2015). arXiv:1504.04632
178. S.A. Usman, et al., Class. Quantum Grav. **33**(21), 215004 (2016). DOI 10.1088/0264-9381/33/21/215004. arXiv:1508.02357
179. M. Vallisneri, J. Kanner, R. Williams, A. Weinstein, B. Stephens, J. Phys. Conf. Ser. **610**(1), 012021 (2015). DOI 10.1088/1742-6596/610/1/012021. arXiv:1410.4839
180. T. Dal Canton, et al., Phys. Rev. D **90**(8), 082004 (2014). DOI 10.1103/PhysRevD.90.082004. arXiv:1405.6731
181. K. Cannon, et al., Astrophys. J. **748**, 136 (2012). DOI 10.1088/0004-637X/748/2/136. arXiv:1107.2665
182. S. Privitera, et al., Phys. Rev. D **89**(2), 024003 (2014). DOI 10.1103/PhysRevD.89.024003. arXiv:1310.5633

183. S. Klimenko, et al., Phys. Rev. D **93**(4), 042004 (2016). DOI 10.1103/PhysRevD.93.042004. arXiv: 1511.05999
184. R. Lynch, S. Vitale, R. Essick, E. Katsavounidis, F. Robinet, Phys. Rev. D **95**(10), 104046 (2015). DOI 10.1103/PhysRevD.95.104046
185. T.B. Littenberg, N.J. Cornish, Phys. Rev. D **91**(8), 084034 (2015). DOI 10.1103/PhysRevD.91.084034. arXiv:1410.3852
186. J. Abadie, et al., Phys. Rev. D **85**, 082002 (2012). DOI 10.1103/PhysRevD.85.082002. arXiv: 1111.7314
187. C.P.L. Berry, et al., Astrophys. J. **804**(2), 114 (2015). DOI 10.1088/0004-637X/804/2/114. arXiv: 1411.6934
188. J. Veitch, et al., Phys. Rev. D **91**(4), 042003 (2015). DOI 10.1103/PhysRevD.91.042003. arXiv: 1409.7215
189. L.P. Singer, L.R. Price, Phys. Rev. D **93**(2), 024013 (2016). DOI 10.1103/PhysRevD.93.024013. arXiv:1508.03634
190. S. Fairhurst, New J. Phys. **11**, 123006 (2009). DOI 10.1088/1367-2630/11/12/123006. arXiv: 0908.2356. [Erratum: New J. Phys.13,069602(2011)]
191. S. Fairhurst, Class. Quantum Grav. **28**, 105021 (2011). DOI 10.1088/0264-9381/28/10/105021. arXiv:1010.6192
192. S. Vitale, M. Zanolin, Phys. Rev. D **84**, 104020 (2011). DOI 10.1103/PhysRevD.84.104020. arXiv: 1108.2410
193. S. Vitale, et al., Phys. Rev. D **85**, 064034 (2012). DOI 10.1103/PhysRevD.85.064034. arXiv: 1111.3044
194. S. Nissanke, J. Sievers, N. Dalal, D. Holz, Astrophys. J. **739**, 99 (2011). DOI 10.1088/0004-637X/ 739/2/99. arXiv:1105.3184
195. L.P. Singer, et al., Astrophys. J. **795**(2), 105 (2014). DOI 10.1088/0004-637X/795/2/105. arXiv: 1404.5623
196. K. Grover, et al., Phys. Rev. D **89**(4), 042004 (2014). DOI 10.1103/PhysRevD.89.042004. arXiv: 1310.7454
197. S. Chatterji, et al., Phys. Rev. D **74**, 082005 (2006). DOI 10.1103/PhysRevD.74.082005. arXiv: gr-qc/0605002
198. H. Dimmelmeier, C. Ott, A. Marek, H.T. Janka, Phys. Rev. D **78**, 064056 (2008). DOI 10.1103/ PhysRevD.78.064056. arXiv:0806.4953
199. C. Ott, Class. Quantum Grav. **26**, 063001 (2009). DOI 10.1088/0264-9381/26/6/063001. arXiv: 0809.0695
200. K. Yakunin, et al., Class. Quantum Grav. **27**, 194005 (2010). DOI 10.1088/0264-9381/27/19/194005. arXiv:1005.0779
201. C. Ott, et al., Phys. Rev. Lett. **106**, 161103 (2011). DOI 10.1103/PhysRevLett.106.161103. arXiv: 1012.1853
202. R. Essick, S. Vitale, E. Katsavounidis, G. Vedovato, S. Klimenko, Astrophys. J. **800**(2), 81 (2015). DOI 10.1088/0004-637X/800/2/81. arXiv:1409.2435
203. C. Cutler, E.E. Flanagan, Phys. Rev. D **49**, 2658 (1994). DOI 10.1103/PhysRevD.49.2658. arXiv: gr-qc/9402014
204. S. Nissanke, D.E. Holz, S.A. Hughes, N. Dalal, J.L. Sievers, Astrophys. J. **725**, 496 (2010). DOI 10.1088/0004-637X/725/1/496. arXiv:0904.1017
205. J. Aasi, et al., Phys. Rev. D **88**, 062001 (2013). DOI 10.1103/PhysRevD.88.062001. arXiv:1304.1775
206. A. Vecchio, Phys. Rev. D **70**, 042001 (2004). DOI 10.1103/PhysRevD.70.042001. arXiv:astro-ph/ 0304051
207. M.V. van der Sluys, et al., Astrophys. J. Lett. **688**, L61 (2008). DOI 10.1086/595279. arXiv:0710.1897
208. S. Vitale, R. Lynch, J. Veitch, V. Raymond, R. Sturani, Phys. Rev. Lett. **112**(25), 251101 (2014). DOI 10.1103/PhysRevLett.112.251101. arXiv:1403.0129
209. B. Farr, et al., Astrophys. J. **825**(2), 116 (2016). DOI 10.3847/0004-637X/825/2/116. arXiv: 1508.05336
210. C. Hanna, I. Mandel, W. Vousden, Astrophys. J. **784**, 8 (2014). DOI 10.1088/0004-637X/784/1/8. arXiv:1312.2077
211. X. Fan, C. Messenger, I.S. Heng, Astrophys. J. **795**(1), 43 (2014). DOI 10.1088/0004-637X/795/1/43. arXiv:1406.1544
212. L. Blackburn, et al., Astrophys. J. Suppl. **217**(1), 8 (2015). DOI 10.1088/0067-0049/217/1/8. arXiv: 1410.0929

213. L.P. Singer, et al., Astrophys. J. Lett. **829**(1), L15 (2016). DOI 10.3847/2041-8205/829/1/L15. arXiv:1603.07333
214. J. Abadie, et al., Astrophys. J. **760**, 12 (2012). DOI 10.1088/0004-637X/760/1/12. arXiv:1205.2216
215. J. Aasi, et al., Phys. Rev. Lett. **113**(1), 011102 (2014). DOI 10.1103/PhysRevLett.113.011102. arXiv:1403.6639
216. J. Aasi, et al., Phys. Rev. D **89**(12), 122004 (2014). DOI 10.1103/PhysRevD.89.122004. arXiv:1405.1053
217. H.Y. Chen, D.E. Holz. Facilitating follow-up of LIGO–Virgo events using rapid sky localization (2015). arXiv:1509.00055
218. L.P. Singer, et al., Astrophys. J. Suppl. **226**(1), 10 (2016). DOI 10.3847/0067-0049/226/1/10. arXiv:1605.04242
219. P. Jaranowski, A. Królak, Living Rev. Rel. **15**, 4 (2012). DOI 10.12942/lrr-2012-4. arXiv:0711.1115
220. B. Abbott, et al., Phys. Rev. X **6**(4), 041014 (2016). DOI 10.1103/PhysRevX.6.041014. arXiv:1606.01210
221. I. Mandel, R. O'Shaughnessy, Class. Quantum Grav. **27**, 114007 (2010). DOI 10.1088/0264-9381/27/11/114007. arXiv:0912.1074
222. P. Canizares, S.E. Field, J.R. Gair, M. Tiglio, Phys. Rev. D **87**(12), 124005 (2013). DOI 10.1103/PhysRevD.87.124005. arXiv:1304.0462
223. M. Pürrer, Class. Quantum Grav. **31**(19), 195010 (2014). DOI 10.1088/0264-9381/31/19/195010. arXiv:1402.4146
224. P. Canizares, et al., Phys. Rev. Lett. **114**(7), 071104 (2015). DOI 10.1103/PhysRevLett.114.071104. arXiv:1404.6284
225. R. Smith, et al., Phys. Rev. D **94**(4), 044031 (2016). DOI 10.1103/PhysRevD.94.044031. arXiv:1604.08253
226. S. Vinciguerra, J. Veitch, I. Mandel, Class. Quantum Grav. **34**(11), 115006 (2017). DOI 10.1088/1361-6382/aa6d44. arXiv:1703.02062
227. T. Sidery, et al., Phys. Rev. D **89**(8), 084060 (2014). DOI 10.1103/PhysRevD.89.084060. arXiv:1312.6013
228. B.F. Schutz, Class. Quantum Grav. **28**, 125023 (2011). DOI 10.1088/0264-9381/28/12/125023. arXiv:1102.5421
229. S.M. Gaebel, J. Veitch, Class. Quant. Grav. **34**(17), 174003 (2017). DOI 10.1088/1361-6382/aa82d9. arXiv:1703.08988
230. B.P. Abbott, et al., Phys. Rev. D **95**(6), 062003 (2017). DOI 10.1103/PhysRevD.95.062003. arXiv:1602.03845
231. B. Bécsy, et al., Astrophys. J. **839**, 1 (2016). DOI 10.3847/1538-4357/aa63ef. arXiv:1612.02003
232. S. Klimenko, S. Mohanty, M. Rakhmanov, G. Mitselmakher, Phys. Rev. D **72**, 122002 (2005). DOI 10.1103/PhysRevD.72.122002. arXiv:gr-qc/0508068
233. S. Vitale, et al., Mon. Not. R. Astron. Lett. **466**(1), L78 (2016). DOI 10.1093/mnrasl/slw239. arXiv:1611.02438
234. J. Abadie, et al. Sensitivity Achieved by the LIGO and Virgo Gravitational Wave Detectors during LIGO's Sixth and Virgo's Second and Third Science Runs (2012). arXiv:1203.2674
235. P. Sutton. A rule of thumb for the detectability of gravitational-wave bursts (2013). arXiv:1304.0210
236. A. Staley, et al., Class. Quantum Grav. **31**(24), 245010 (2014). DOI 10.1088/0264-9381/31/24/245010
237. E.J. Daw, J.A. Giaime, D. Lormand, M. Lubinski, J. Zweizig, Class. Quantum Grav. **21**, 2255 (2004). DOI 10.1088/0264-9381/21/9/003. arXiv:gr-qc/0403046
238. L. Barsotti, P. Fritschel, Early aLIGO configurations: example scenarios toward design sensitivity. Tech. Rep. LIGO-T1200307-v4, Pasadena, CA (2012). URL `https://dcc.ligo.org/LIGO-T1200307/public`
239. J. Aasi, et al., Astrophys. J. Suppl. **211**, 7 (2014). DOI 10.1088/0067-0049/211/1/7. arXiv:1310.2314
240. M.M. Kasliwal, S. Nissanke, Astrophys. J. Lett. **789**, L5 (2014). DOI 10.1088/2041-8205/789/1/L5. arXiv:1309.1554
241. P.A. Evans, et al., Mon. Not. Roy. Astron. Soc. **455**, 1522 (2016). DOI 10.1093/mnras/stv2213. arXiv:1506.01624
242. N. Gehrels, et al., Astrophys. J. **820**(2), 136 (2016). DOI 10.3847/0004-637X/820/2/136. arXiv:1508.03608
243. S. Ghosh, S. Bloemen, G. Nelemans, P.J. Groot, L.R. Price, Astron. Astrophys. **592**, A82 (2016). DOI 10.1051/0004-6361/201527712. arXiv:1511.02673
244. M.L. Chan, Y.M. Hu, C. Messenger, M. Hendry, I.S. Heng, Astrophys. J. **834**, 84 (2017). DOI 10.3847/1538-4357/834/1/84. arXiv:1506.04035

245. O.S. Salafia, et al. Where and when: optimal scheduling of the electromagnetic follow-up of gravitational-wave events based on counterpart lightcurve models (2017). arXiv:1704.05851
246. L.P. Singer, in *LIGO-DAWN Workshop II: What's next for LIGO?* (2016). URL `https://dcc.ligo.org/LIGO-G1601468/public`
247. *What's next for LIGO? Report from the 2nd Dawn Workshop 7-8 July 2017, Georgia Tech, Atlanta, GA*. URL `https://dcc.ligo.org/LIGO-P1600350/public`
248. P.A.R. Ade, et al., Astron. Astrophys. **594**, A13 (2016). DOI 10.1051/0004-6361/201525830. arXiv: 1502.01589